THE INTERACTION OF IO AND THE JOVIAN MAGNETIC FIELD:

IO'S ALFVEN WINGS AND PARTICLE ACCELERATION.

By

Vincent Dols

RECOMMENDED: _____

_____

_____

_____

_____
Advisory Committee Chair

_____
Department Head

APPROVED: _____
Dean, College of Science, Engineering and Mathematics

_____
Dean of the Graduate School

_____
Date

THE INTERACTION OF IO AND THE JOVIAN MAGNETIC FIELD:

IO'S ALFVEN WINGS AND PARTICLE ACCELERATION.

A

THESIS

Presented to the Faculty

of the University of Alaska Fairbanks

in Partial Fulfillment of the Requirements

for the Degree of

MASTER IN SPACE PHYSICS

By

Vincent Dols, Licencié en Sciences Physiques

Fairbanks, Alaska

August 2001

Abstract

Conditions for the formation of an electric field along the field lines of Jupiter crossing the satellite Io are investigated by examining the properties of Io's Alfven wave.

A three-dimensional self-consistent MHD model, using a simplified magnetosphere description, illustrates the formation of this electric field and of the Io's related auroral emission in the Jovian ionosphere.

The Alfven wing properties between Io and Jupiter are studied with a one-dimensional MHD model and a realistic magnetosphere. Any change in the Io/Jupiter system affects the structure of the Alfven wing and likely affects the structure of Io's auroral emission. This emission is likely structured in multi-spots and the angle between the first spot and the instantaneous projection of Io is less than 3^0. In the limited context of the 1D approximation, the acceleration mechanism is expected close to Jupiter.

Table of contents

List of figures

List of tables

Acknowledgments

I would like to thank the people that helped me with this work. First, I thank my advisor Antonius Otto for his continual support, infinite patience, unlimited availability, human qualities, impressive scientific knowledge and insights. I hope that these words express correctly how grateful I am. But his coffee is definitely too strong for me. I thank also my committee members Dirk Lummerzheim, David Newman, Hans Nielsen and John Olson for their flexibility and meaningful comments on my work.

I am also grateful to Peter Delamare for his support and scientific comments, to Fran Bagenal who provided the plasma density and magnetic field strength along the Io field-lines used in this work, to John Clarke for providing unpublished information about the Io multi-spot observations with the Hubble Space Telescope, to Jack Connerney for pointing the infrared multi-spot observation article to my attention and to Chris who helped me using the IARC printers and computers. Thanks to Cecile who helped me so much when I needed to print the thesis and get the figures presented in this work in the correct format.

Thanks to all the friends, colleagues and teachers who made my stay in Alaska a great experience.

CHAPTER 1: INTRODUCTION

What is the phenomenon to be explained?

Jupiter's magnetosphere is in many ways a unique object in the solar system. The Galilean satellite Io is deeply embedded in the magnetosphere and is thought to be a substantial source of plasma in the Jovian magnetosphere. Jupiter's magnetospheric dynamics is very different from the Earth's because of the strong magnetic moment of the planet and its fast rotation. In this work, we will focus on the inner part of the magnetosphere, close to the orbit of the first Galilean satellite Io, at 6 Jovian radii from Jupiter. When the Voyager 1 probe passed close to the Io's surface, in 1979, it spotted many active volcanoes, spewing sulfur and oxygen compounds at altitudes as high as 300km. Some of this material escapes the satellite and becomes ionized, feeding a huge plasma torus encircling Jupiter like a giant doughnut. Most of this plasma will eventually diffuse throughout the magnetosphere. The torus, embedded in the Jovian magnetic field, corotates with Jupiter, with a period of about 10 hours while Io's orbital period is much longer: about 42 hours. Io is thus swept by the torus' plasma, which leads to further ionization of the neutrals around Io.

In 1964, studies of radio emissions from Jupiter demonstrated the strong electromagnetic coupling of Io and the Jovian magnetic field. This interaction is dramatically illustrated by recent ultraviolet and infrared imaging of Jupiter's ionosphere. Figure 1 shows an ultraviolet picture taken by the Space Telescope Imaging Spectrograph (STIS) aboard the Hubble Space Telescope (HST) in 1998. The bright high latitude structures are emissions of molecular hydrogen excited by impact of impinging magnetospheric particles. Figure 2 is an infrared image of the ionosphere of Jupiter taken with NASA's Infrared Telescope Facility (IRTF) at Mauna Kea in 1995. It shows the thermal emission of H_3^+ formed by molecular hydrogen ionized by impinging particles.

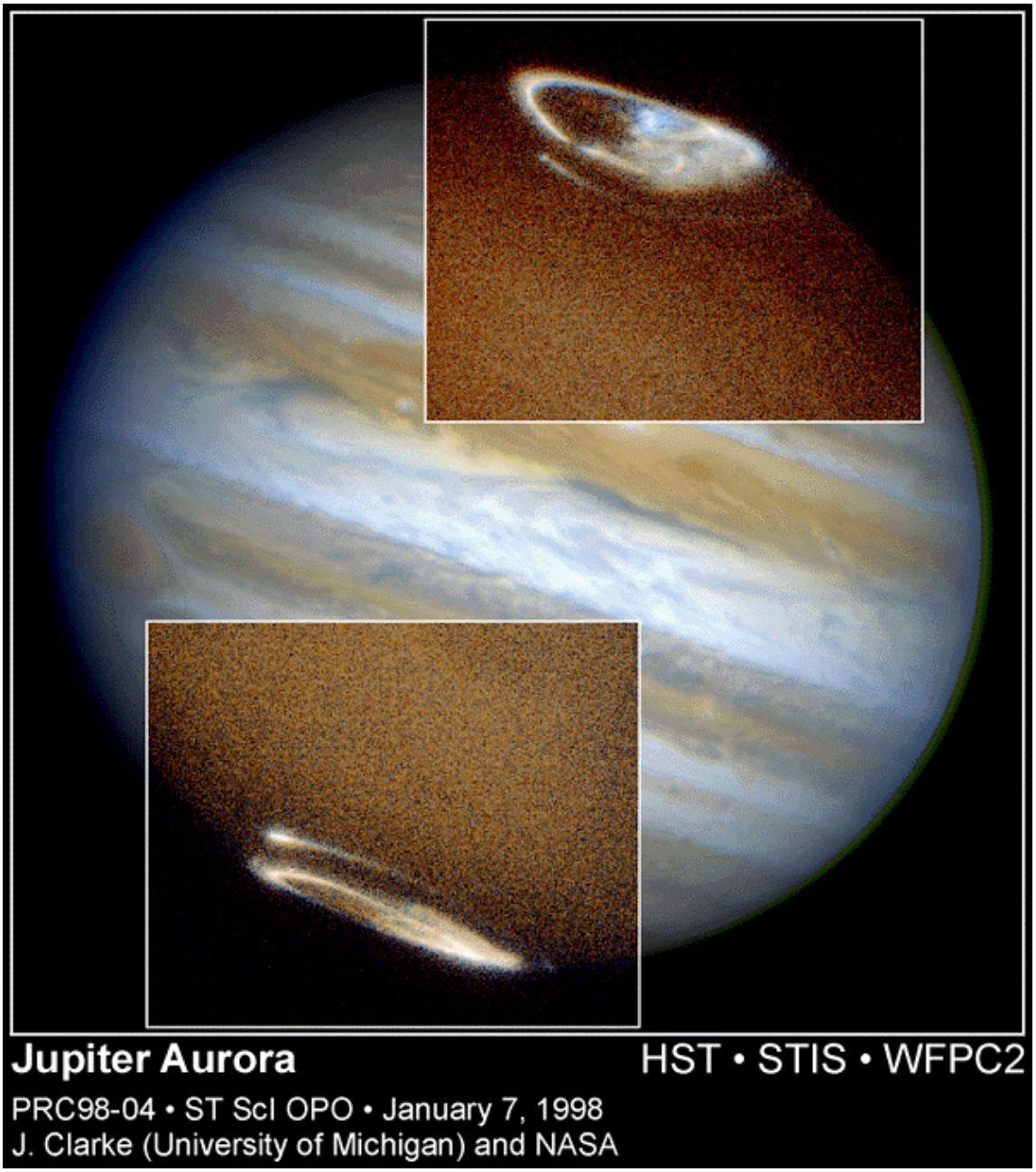

Figure 1: Ultraviolet image of the aurora and the Io footprint auroral emissions.

This image is taken in the ultraviolet by the STIS camera onboard the Hubble Space Telescope (Clarke, STScI)

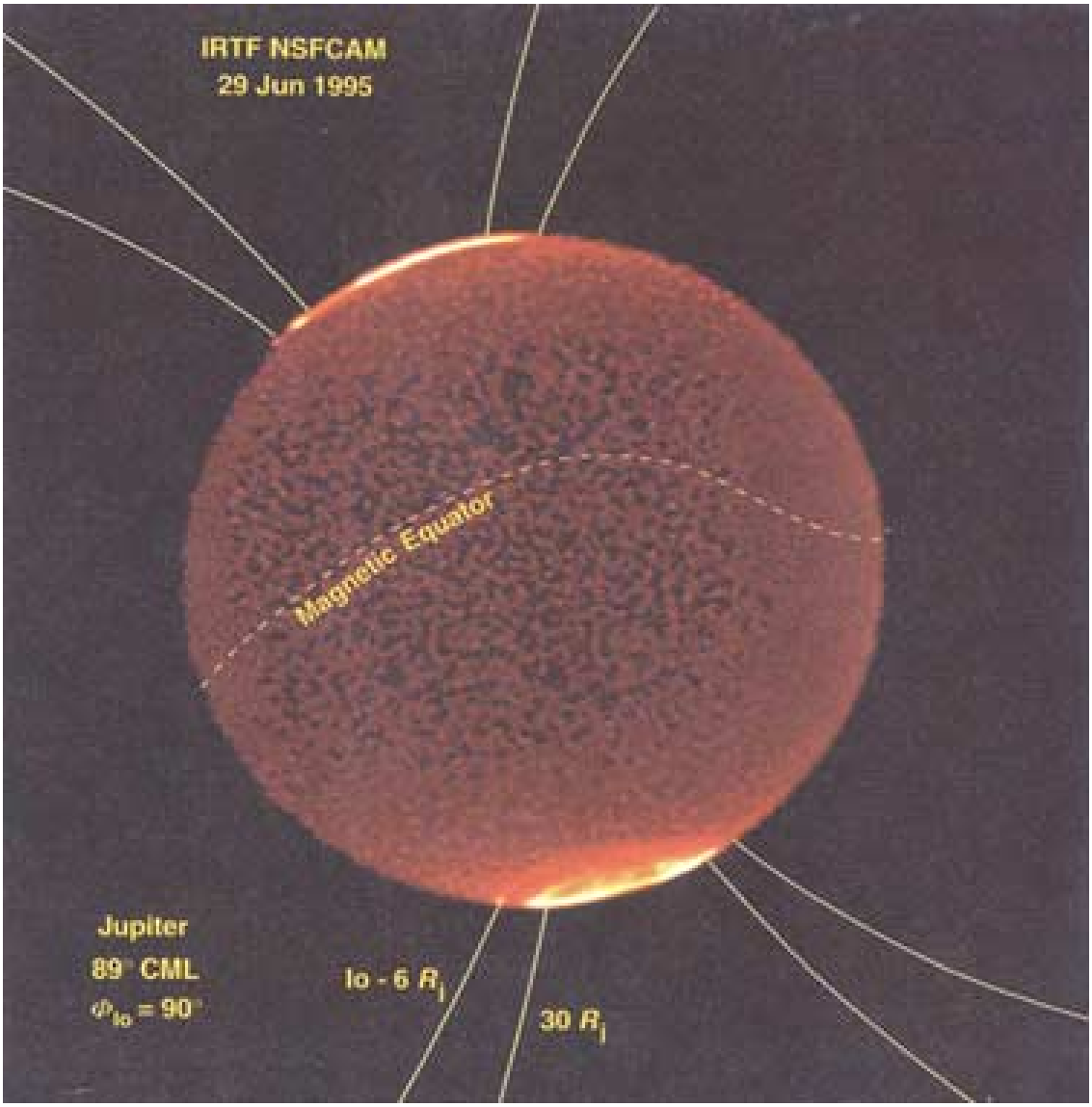

Figure 2: Infrared image at 3.4 μm of the aurora and the Io footprint emissions. This image is obtained at NASA's IRTF at Mauna Kea, Hawaii, using the NSFCAM facility imager (Connerney and Satoh, 2000).

Both images display the same features in the two hemispheres: a high latitude auroral oval probably connected to the far/middle magnetosphere and, about 8^{o} below the auroral oval, a spot followed by a long trailing tail. Using a model of the Jovian magnetic field, it was shown that the spot and tail map close to the Io location in its orbit and result from the Io/Jupiter interaction. Spectral analyses of the spot and its tail show that the impinging particles might have energy of a

few keV if electrons are assumed. The electrons close to Io are pretty cold (about 5 eV) and it is clear that some acceleration mechanism must be at work along the field lines crossing Io. The Io/Jupiter electromagnetic interaction has been studied since 1964, but most of this interaction is still poorly understood. The nature of the impinging particles (ions or electrons) and the acceleration mechanism are unknown.

What is the contribution of this thesis?

The contribution of this thesis is the study, through numerical simulations, of one possible acceleration mechanism: The formation of a localized electric field parallel to the Jovian field lines ($\boldsymbol{E}_{//}$) associated with the Alfven wave magnetic perturbations created by the relative motion of Io in the plasma torus. This parallel electric field could accelerate particles to a few tens of keV and precipitate them in the Jovian ionosphere. In this work, the formation of a parallel electric field is intimately connected to the appearance of a localized resistivity along the field lines where the Alfven wave propagates. Eventually, the parallel electric field leads to a reconfiguration of the field line topology. The topology change is not a central issue in this work, but for simplicity and because of these last two reasons, we will call this whole process "resistive reconnection" in the rest of the thesis. Io, because of its interaction with the torus and because of the observation of Io's related auroral emissions, is a perfect model case for this mechanism. The relevance of this mechanism will be discussed in the next chapters but it should be stated immediately that the precise physics of the source for the parallel electric field is beyond the scope this work. When needed, the resistivity will be prescribed.

We will first show the $\boldsymbol{E}_{//}$ formation mechanism associated with the reconnection process using a three dimensional magnetohydrodynamic (3D MHD) model but our main focus will be the study of the properties of the **Alfven wave propagation** and the **conditions** for the parallel electric field formation.

The outline of the thesis is as follows:

In **Chapter2** we describe the magnetosphere of Jupiter close to Io.

In **Chapter 3** we review the Io/Jupiter interaction models that have been proposed so far and some of the observations that support these models.

In **Chapter 4** we present the first step in our study of the reconnection process through numerical simulation. We use a three-dimensional numerical model to solve the MHD equations of the

plasma in the torus, from Io to the Jovian magnetosphere. In these simulations, as stated before, the resistivity is prescribed. These simulations show that the model reproduces some of the features observed close to Io and that the Io-related emissions in the Jovian ionosphere can be accounted for by the resistive reconnection processes. This 3D model, because of its complexity, has a relatively low spatial resolution and uses a simplified description of the magnetosphere: the magnetic field of Jupiter and plasma density along the field line crossing Io are assumed to be uniform. A comprehensive 3D modeling featuring a realistic description of the magnetosphere seems to be the ultimate goal of the study of the interaction but is beyond the scope of the present work. However, important physical mechanisms can be studied and understood using simple models. This is the goal we pursue in the next chapters.

In **Chapter 5**, we use a one-dimensional model to study the effect of a realistic magnetic field and torus density parameterization on the Io/Jupiter interaction. This chapter focuses on the propagation of an Alfven wave created by the Io/torus interaction. The 1D model naturally provides a 2D mapping (along field line and along Io's orbit), which nicely illustrates the Alfven wave propagation.

In **Chapter 6** we use this 2D mapping to study the onset conditions for a parallel electric field: The associated reconnection process is not modeled per se but we analyze where anomalous resistivity is likely to form and how the acceleration efficiency varies along the field lines.

The **Chapter 7** summarizes this work.

CHAPTER 2: THE MAGNETOSPHERE OF JUPITER

A complete review of the Jovian magnetosphere after the Voyager flyby can be found in Dessler (1983) and included references. This chapter describes briefly the magnetosphere of Jupiter close to Io. Of particular relevance for the rest of the thesis are the Jovian magnetic field modeling, the torus density profile and the neutral cloud where ionization occurs, as we will use these parameters in the simulations of chapter 4 and 5.

2. 1. The Jovian magnetic field

Jupiter's magnetic moment is fairly large, about 4.3 Gauss-R_j^3. The dipole is not aligned with the rotation axis: It is tilted by 9.6^o towards the longitude 202^o in the northern hemisphere (in the usual system III (1965) longitude system, Dessler, 1985). It possesses substantial quadrupole and octupole moments. The internally produced field dominates the inner magnetosphere out to a distance of 6 Jovian Radii (R_j), the orbital distance of Io. The middle magnetosphere of Jupiter extends from 6 to 30-50 R_j. It is dominated by an equatorial azimuthal current disc that stretches the field lines in the radial direction. The sunward magnetopause distance is highly variable (from 45 to 100 $R_{j)}$ and the magnetotail might extend at least beyond the orbit of Saturn.

The details of a planet's magnetic field are determined by fitting magnetometer data obtained along spacecraft trajectories using a spherical harmonic expansion model with or without external current sources. Based on the Voyager 1 and Pioneer 11 observations, Connerney et al. (1981) modeled the magnetosphere for r< 30 Rj where the field due to magnetopause currents is negligible. Their model is azimuthally symmetric. It combines a spherical harmonic model of the internal planetary field developed to the octupole term with an explicit model of the magnetodisc current system. The current disc is modeled as a finite thickness (5 Rj) annular current sheet extending from 5 to 50 Rj in the magnetic equatorial plane. This combined model is usually referred to as the GSFCO4 + magnetodisc model (for Goddard Space Flight Center and development to 4th order of the internal field). Later on, Connerney developed the same model to

the sixth order (GSFCO6 model) to show the sensitivity to higher order terms (Connerney, 1992). The magnetic field data set is limited by the trajectory of the small number of probes launched at Jupiter, consequently the accuracy of the internal field model was a serious limitation, leading to uncertainty of about 10^{o} latitude in the mapping on the surface of Jupiter of different regions of the Jupiter magnetosphere (Connerney and Satoh, 2000). Recently, the discovery of the emission feature at the instantaneous foot of the Io Flux Tube (IFT) in ultraviolet and infrared images (Figure 1 and Figure 2) added a new constraint close to the planet that cannot be sampled by any spacecraft. This feature provides an unambiguous reference on Jupiter's surface through which magnetic field lines with an equatorial crossing distance ~6 Rj must pass. Connerney et al. (1998) developed a new version of the magnetic field model called VIP4 (for Voyager, Pioneer and Io and fourth order development of the internal field) that provides a mapping accuracy of 1-2^{o} at Io's footprint latitude (Connerney and Satoh, 2000) (Figure 3).

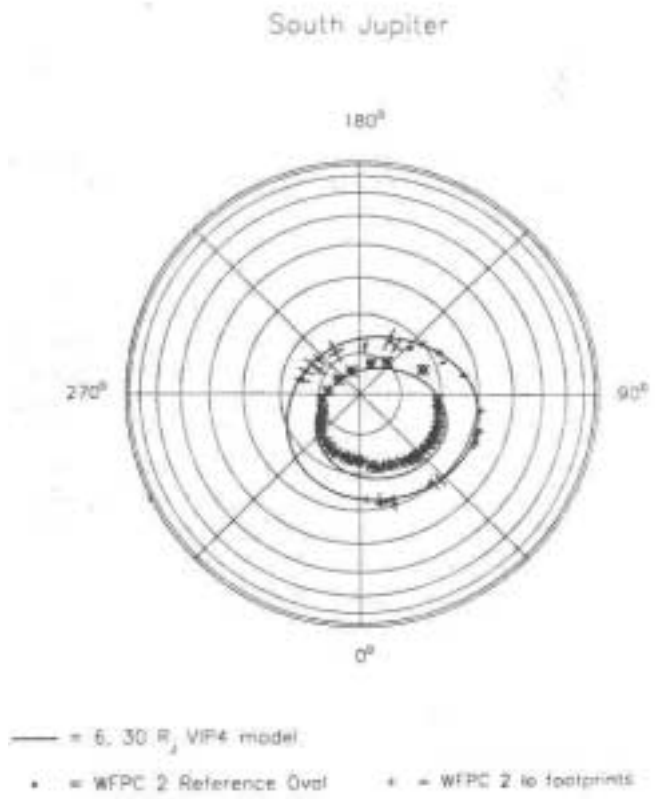

Figure 3: VIP4 planetary magnetic field model.

South pole projection of the footprint (solid lines) of the field lines crossing the Jovian equatorial plane at a distance of 6Rj (Io's orbit) and 30 Rj in the VIP4 model. Crosses indicate the location of Io auroral spots observed by the WFPC2 (continued next page)

camera aboard HST. The lengths of the lines indicate measurement uncertainties. The stars represent the location of the observed high latitude auroral emissions unrelated to Io and not relevant for the present work (from Clarke et al., 1996).

The GSFCO6 and VIP4 model are usually referred to in the most recent articles about the imaging of the footprint of the Io flux tube (see chapter 3).

In this thesis, no mapping is involved. In chapter 4 and 5, we simply need the variation of the field strength along the field line and for this purpose, the GSFCO4 + magnetodisc model is good enough. This variation along the field line crossing Io (distance~ 5.9 Rj) as modeled by the GSFCO4 + magnetodisc is illustrated on Figure 21 and compared to a dipole magnetic field.

2. 2. Io and its neutral clouds

Io is the first Galilean moon of Jupiter. Io orbits around Jupiter at a distance ~5.9 Rj. Its radius is about 1,820 km (Jupiter's radius ~71,400km ~40 R_{Io}). The length of the field line, from Io to the Jovian ionosphere is about 280 R_{Io}. The question of whether Io has an internal magnetic field has been a continuing issue since the Voyager 1 flyby that has been reactivated by the recent Galileo flyby (Khurana et al., 1997).

During its flyby, Voyager 1 discovered an impressive volcanic activity that expels oxygen and sulfur compounds to altitude as high as 300 km. An SO_2 atmosphere was detected around Io. The two sources of this atmosphere are thought to be the active volcanic plumes and sunlit sublimation of SO_2 frost that has fallen back to Io's surface. The picture is thus a collisionally thick (10^{16} SO_2 cm^{-2}), probably patchy SO_2 atmosphere showing temporal variation depending on the volcanic activity and sunlit illumination (Wong et al., 2000). The relative composition of Io's atmosphere is not well known but SO, O, S, and O_2 are expected to be created from SO_2 by the photo- and gas-phase chemistry.

In addition, huge neutral clouds of Na, K, (although thought to be minor components of the volcanic plumes) O and S have been detected extending far from Io. The Na cloud extends to distance of hundreds of Rj (Smyth, 1992) and Roesler et al., 1999 shows neutral oxygen and sulfur cloud densities extending to a distance of 20 R_{Io}. These neutrals are ionized by collisions with the magnetospheric plasma or by the UV solar radiation and feed a huge Io plasma torus at a rate of about 1 ton of material per second. Although the neutral clouds are pretty extended, it is

thought that the major ionization takes place close to Io although the location is still an issue. It is reasonable to think that ionization occurs at a distance of about 1-2 R_{Io} from the surface, where the neutral density is the largest (Bagenal, 1997). This ionization volume will be used for the numerical simulations in chapter 4.

2. 3. The Io plasma torus

When Voyager 1 approached Jupiter, the ultraviolet spectrometer detected powerful emission from sulfur and oxygen ions in a toroidal region encompassing the orbit of Io (Figure 4). The Plasma Science instrument made local measurements of both electrons and various ionic species: O^+, O^{++}, S^+, S^{++}, S^{+++}, SO_2^+ or S_2^+. The strong centrifugal force confines the plasma close to the region of the field line most distant from Jupiter's spin axis: the centrifugal equator. The centrifugal equator is close to the magnetic equator, it is tilted by ~7° relative to the plane of the orbit of Io (Bagenal and Sullivan, 1981).

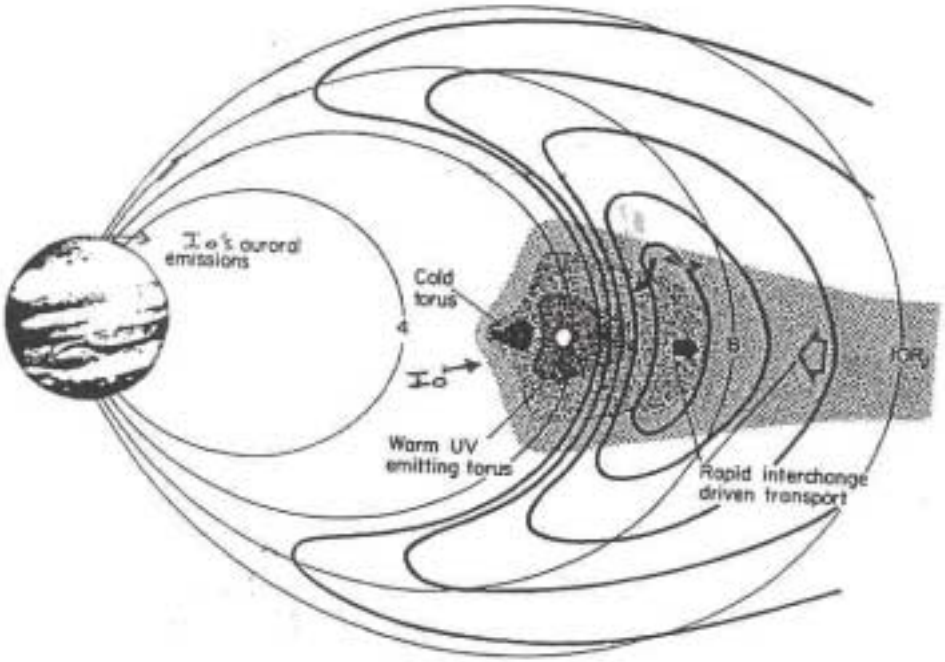

Figure 4: Sketch of Jupiter and its plasma torus.
(Adapted from Thorne, 1983)

Figure 5 shows the structure of the torus as modeled by Bagenal (1994) based on Voyager measurements. The torus presents 3 main structures:

- **The cold torus** extends from 5.3 Rj to 5.6 Rj, the dominant ions are S^+ (70 %) and O^+ (20%), the electron density is peaking at 1000 e^-/cm^3 and the temperatures are cold: $T_e \sim 1eV$ and $T_i \sim 1eV$.

- **The warm torus** extends roughly from 5.6 to 8 Rj. Io's orbit is embedded in the warm torus at a distance ~5.9 RJ. The main ions are O^+ (40%), S^{++} (20%) and S^+ (10%), the electron density peaks at about 2000 e^-/cm^3 and the mass density at 57,000 amu/cm^3 , close to the orbit of Io. The ion temperature is about 60 eV and the electron temperature is ~5 eV

- **In between** the cold and warm torus, Voyager detected a thin structure with a high electron density (3000 e^-/cm^3): Because of its narrow shape, it is called **the ribbon**. It is ~0.2Rj thick and 0.5 Rj high and its location varies between 5.6 and 5.9 Rj.

The torus observed 16 years later by the Galileo probe, in 1995, seems to be a little bit different: the ribbon seemed to have disappeared or at least, shifted in the wake of Io when Galileo flew through. The peak electron density in the warm torus was ~4000 e^-/cm^3, twice as large as the one measured by Voyager 1 on a similar trajectory, out of the ribbon.

We will use the Bagenal (1994) torus density profile along the field line in the numerical simulations presented on chapter 4 and 5. The plasma characteristics observed along the Voyager trajectory were extrapolated along the field lines by numerically solving the equations of diffusive equilibrium, taking the centrifugal force into account, to produce radial profiles of electrons and ions densities. The Voyager 1 probe did not detect any protons, because of the 10 eV threshold of the Plasma Science instrument onboard Voyager I (Crary et al., 1996) but the author added about 10% of protons to the heavy ion density as suggested by whistler measurements. The torus density profile along the Io's field line will be shown on Figure 20.

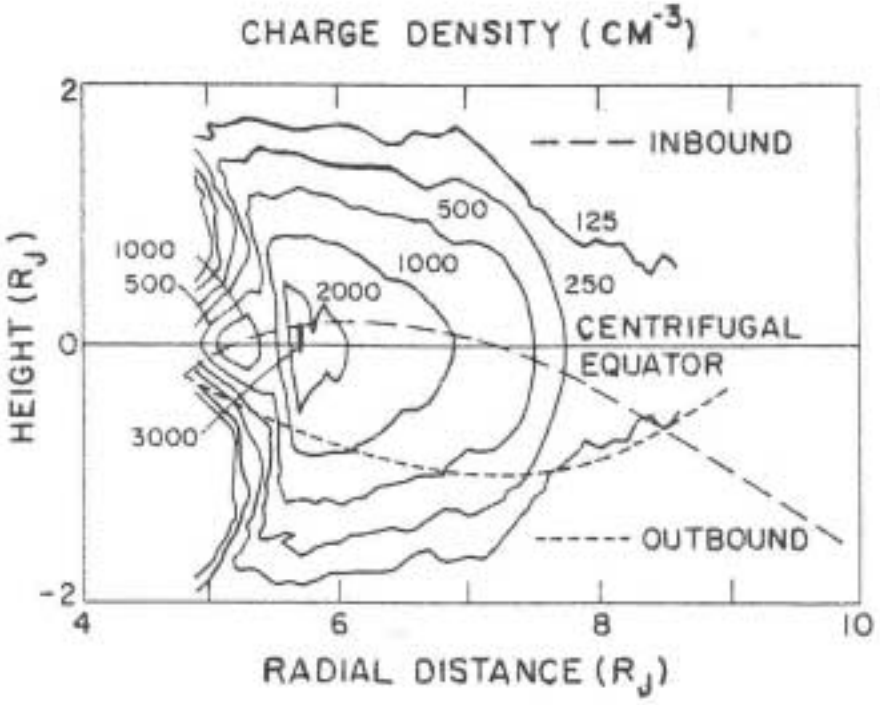

Figure 5: Torus electron density contour lines.

From Voyager-based model in centrifugal coordinates based on the GSFCO4 magnetic field model. The trajectory of Voyager is shown in dashed lines (from Bagenal et al., 1994)

The torus plasma is frozen to the Jovian magnetic field and spins around Jupiter in about 10 hours. Io's orbit is much slower: its orbital period is about 42 hours. Thus the plasma of the torus and the Jovian magnetic field lines sweep Io at a relative velocity of 57 km/sec. The collisions sputter the neutrals from the patchy, variable atmosphere of Io and are actually the main cause of the neutral ionization. This ionization and the friction between neutrals and plasma are the causes of the magnetic perturbation that we will study in the next chapter. Moreover, the torus orbits in the Jovian centrifugal equator. Because of its tilt, the torus is wobbling rapidly around the Jovian rotational axis. In other words, Io is moving up and down in the torus by a distance of ~1 Rj thereby experiencing very different plasma densities during the 10 hour torus orbit. Thus, the strength of the interaction between Io and the torus is highly variable.

Table 1: Jupiter and Io: selected physical parameters.

(Adapted from Dessler, 1983)

Jupiter

Heliocentric distance	5.20 AU = 7.78×10^8 km
Sidereal period	11.86 years
Synodic period	398.88 days= 13.10 months = 1.092 years
Mean orbital speed	13.06 km/sec = 15.7 Rj/day
Equatorial radius (I Rj)	7.14×10^4 km = 1 Rj (by definition)
Polar radius	6.68×10^4 km
Mass	317.8 M_{Earth} = 1.901×10^{27} kg
Escape speed	61 km/sec
Gravitational acceleration	25.9 m/sec^2 = 2.64 g_{Earth}
Escape energy for Hydrogen atom	19.4 eV
System III (I 965) sidereal spin period	9 hr 55 min 29.71 sec (derived from angular velocity) = 3.573×10^4 sec = 9.925 hr
System III (I 965) angular velocity	1.76×10^{-4} rad/sec = 870.536^o/day (by definition)
Rotational (spin) kinetic energy	3.6×10^{34} J
Spin equator inclined to orbital plane	3^o 5'
Main magnetic-dipole moment	4.2×10^{-4} TRj
Magnetic dipole tilt	$9.8^o \pm 0.3^o$
Tilt toward	$\lambda_{III} = 200^o \pm 2^o$
Dipole displaced	0. 12 ± 0.02 Rj toward $\lambda_{III} = 149^o \pm 6^o$

Io

Jovicentric distance	5.91 Rj = 4.216 x 10^5 km
Sidereal period	1.769 days = 42.46 hr
Mean orbital speed about Jupiter	17.34 km/sec
Angular velocity about Jupiter	4.112 x 10^{-5} rad/sec
Radius	1.82 x 10^3 km = 2.55 x 10^{-2}Rj
Mass	8.91 x 10^{22} kg
Escape speed	2.56 km/sec
Gravitational acceleration	1.80 m/sec^2 = 0.184 g_{Earth}
Corotation speed at Io's orbit	74.2 km/sec
Angular velocity of corotation relative to Io	1.35 x 10^{-4} /sec
Speed of corotation relative to Io	56.8 km/sec
Jovian magnetic field at Io	~2,000 nT
Corotation electric field at Io	0.113 V/m outward from Jupiter
Max potential across Io	411 kV

CHAPTER 3: IO'S INTERACTION IN THE LITERATURE AND SUPPORTING OBSERVATIONS

3. 1. Introduction

The electromagnetic interaction between Io and Jupiter was discovered in 1964 when it appeared that Io modulated the intensity of decametric radio wave (DAM) emitted in the Jupiter's vicinity. Further evidence of this interaction is now available: The in situ detection of a propagating Alfven wave close to the Io flux tube, the infrared (IR) and the ultraviolet (UV) imaging of the ionospheric emissions at the foot of the Io flux tube. These observations are currently interpreted in the frame of two models, the "unipolar inductor model" and the "open-loop Alfven wave model". These two models actually represent two versions of the same interaction between Io and the magnetized torus but none explicitly includes a process that accelerates particles along the field lines. In the following paragraphs, we review briefly the 2 models and the observations that support one or the other. The Io spot/tail observations motivate this work and are described more thoroughly. We will often refer to them in the analysis of our numerical simulation results.

3. 2. Models

The relative motion of Io in the co-rotating plasma torus disturbs the magnetic field of Jupiter. The propagation of this perturbation away from Io is usually described as a propagation of low frequency MHD waves. Most of the energy will propagate along the Io flux tube as Alfven Waves. The magnetic perturbation induces a field-aligned current that propagates down towards the Jovian ionosphere along the Io flux tube. The two models start from there. The difference is the location of the field-aligned current closure. In the unipolar inductor model, the current closes in the Jovian ionosphere as a Pedersen current while in the Alfven Wave model, the current closes at the front of the Alfven Wave, as a polarization current.

3.2.1. The steady state unipolar inductor model

This model was proposed by Goldreich and Lynden-Bell (1969) after the DAM modulation discovery. At that time, the high plasma density of the Io torus had not been discovered yet. It was wrongly assumed that the plasma density close to Io was very low (0.5 cm^{-3}) and consequently, the Alfven speed extremely large. The time for an Alfven wave to go from Io to the Jupiter's ionosphere and back was supposed to be much less than the time required for the plasma to convect past Io (2 R_{Io}/ V_{corot} ~60 sec) so that an Alfven wave emitted by Io would, after reflection on the Jupiter's ionosphere, return back exactly to the location of the moon. After multiple bounces, a steady state would be reached: the entire flux tube would move with a common velocity and a constant DC current would flow through the Io flux tube. This current would be determined entirely by the Io and Jupiter's ionosphere conductivities (Figure 6).

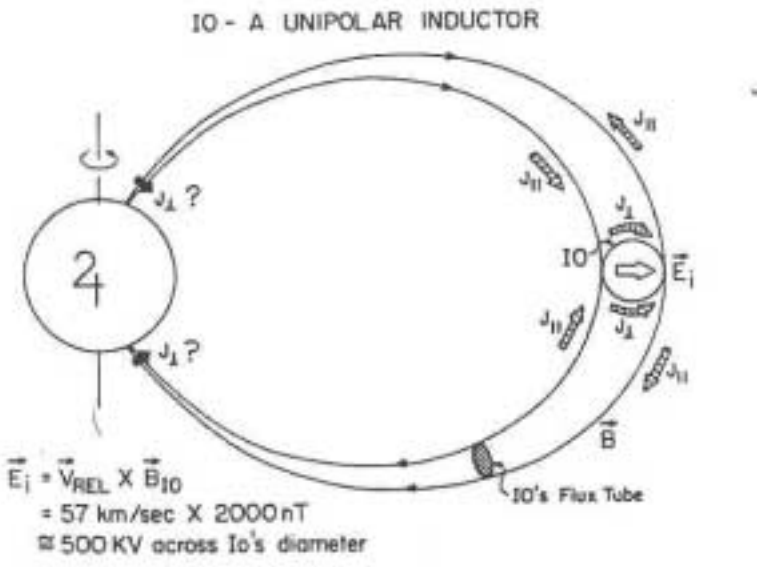

Figure 6: Io as a unipolar inductor.

Schematic representation of the induced current system flowing approximately parallel to the field lines in the Io flux tube. The circuit is closed at the extremes by current flowing in the Jovian ionosphere and in Io (from Acuna et al., 1983)

A prediction of the Goldreich and Lyndel-Bell model, which will be very often referred to in the analysis of the IR or UV Io flux tube footprint images, is the angle of the footprint relative to the instantaneous location of Io projected on Jupiter, called the *lead-angle*. The current flowing in the Io flux tube would twist it so that its foot on the Jovian ionosphere would lead an undisturbed flux tube by ~10^o for every 10^6 amps currents.

3.2.2. The open-loop Alfven wave model

After Voyager 1 went through the torus in 1979, it was clear that the plasma density close to Io was much larger than the one anticipated by Goldreich and Lyndel-Bell. As stated in section 2.2, Voyager 1 measured a plasma density of >2,000 pcl/cm^3 close to the Io's orbit. Consequently, when Io is in the center of the torus, the round trip Alfven propagation time is now estimated at ~1000 sec, much more than the time needed for the plasma to convect past Io so that an Alfven wave launched by Io cannot return back to Io after reflection on the Jovian ionosphere.

When Voyager 1 was close to the Io flux tube, it detected a magnetic perturbation and a plasma density perturbation that were interpreted as an Alfven wave propagating down the field lines. After these observations, theoretical models favored an "open-loop" Io interaction (Neubauer, 1980. Goertz, 1980). The current flowing down to Jupiter's ionosphere is no longer assumed to be constant, but varies along the field line following the Alfven wave. It doesn't close in the Jovian ionosphere, but at the front of the Alfven wave as a polarization current. The Alfven disturbance is confined to "Alfven wings" that make an angle Θ_A (the Mach angle, Dessler, 1985) with the background Jovian magnetic field where $\tan(\Theta_A) = V_{Io} / V_A$. This Mach angle varies with the plasma density and magnetic field along the field lines of Jupiter. The ionospheric foot of the Alfven wing leads Io by an angle called, like in the unipolar inductor model, the ***lead-angle*** that depends on the density of the medium through which it propagates from Io to the ionosphere. For an average Alfven velocity in the torus of about 400 km/s through a path length ~1Rj in the torus, this *lead-angle* would be about 3^o (Connerney et al., 1993) and, for a Voyager-derived torus profile, the *lead-angle* would be < 8^o (Prange et al., 1996). In any case, *the lead-angle* in the open-loop model is thought to be much smaller than in the unipolar inductor model (Connerney and Satoh, 2000).

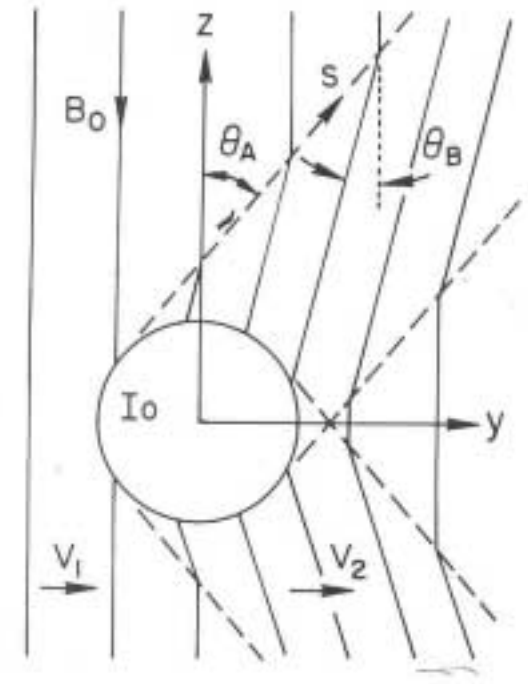

Figure 7: The open-loop Alfven wave model.

Sketch of the magnetic field distortion caused by Alfven waves that are generated by the Io/torus interaction. The waves propagate along the Jovian magnetic field B_0 in the plasma reference frame. These Alfven waves form an Alfven wing whose local angle θ_A to the Jovian magnetic field varies with the local plasma condition (from Hill et al., 1983).

3. 3. Observations supporting the models

3.3.1. The DAM modulation

In 1964, it was shown that high frequency (22 MHz) radio signals from Jupiter were strongly correlated with Io's orbital phase. These radio-emissions are thought to be generated close to the Jovian surface through the cyclotron maser instabilities. Reception is greatly increased when Io's orbital phase (measured from geocentric superior conjunction in the direction of Io's orbital motion) is near 90 or 240°. On one hand, this observation usually favors the unipolar inductor model as it is able to provide a large *lead-angle* close to 15° that would explain the observed

asymmetry in radio emissions. On another hand, the DAM spectra show a "multiple-arc" modulation pattern (arcs in a time-frequency diagram), which are usually interpreted as multiple bounces of standing Alfven waves trapped between the torus and the Jovian ionosphere (Prange et al., 1996. Crary and Bagenal, 1997).

3.3.2. Alfven wave detected by Voyager 1

The Voyager1 encounter with Jupiter had been designed to provide a passage close to the Io's southern Io flux tube. Voyager flew upstream, ~20,500 km under Io as shown in Figure 8. The measurements show a magnetic perturbation of ~100 nT perpendicular to the background Jovian magnetic field, anti-correlated with a perturbation of the ion flux density (Figure 9). This anti-correlation indicates a southward propagation of an Ionian Alfven Wave. From the magnetic perturbation and under some geometrical assumptions, the current flowing through the Io flux tube was computed as ~5 x10^6 amps. (Acuna et al., 1981. Southwood et al., 1980)

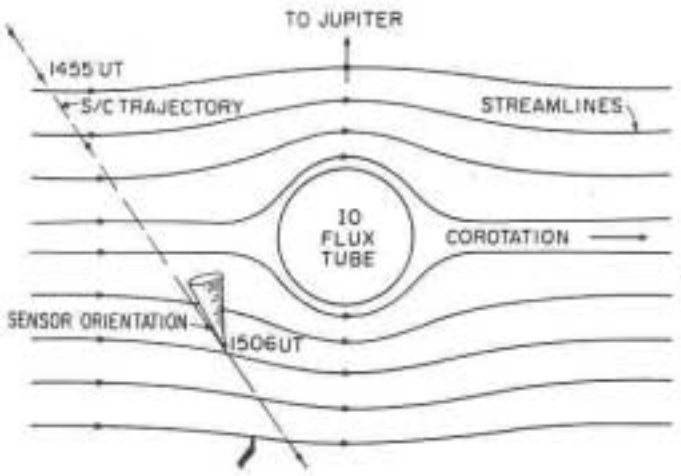

Figure 8: Voyager 1's trajectory close to the Io Flux Tube.
(Belcher, 1983)

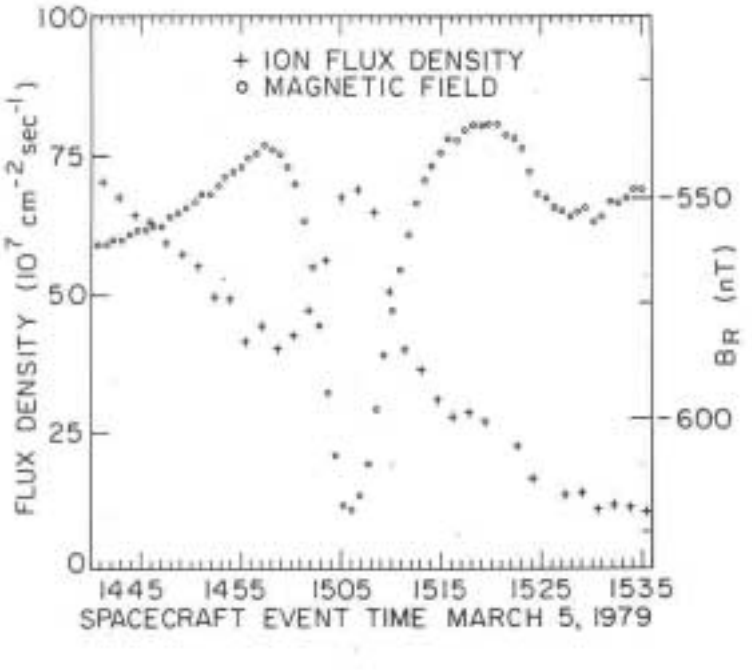

Figure 9: Alfven wave perturbation detected by Voyager close to the Io flux tube. (Belcher, 1983)

3.3.3. Io footprint emission

Recent observations of H_3^+ and H_2 auroral ionospheric emissions at the foot of the Io flux tube provide a new diagnostic of the Io/Jupiter interaction. Figure 2 showed an infrared image of the Io flux tube footprint emission obtained with the IRTF NSFCAM imager from Mauna Kea in Hawaii. It showed the thermal emission of H_3^+, which is formed in the ionosphere by the rapid ion-molecule reaction that follows ionization of H_2 ($H_2^+ + H_2 \rightarrow H_3^+ + H$). The Io footprint is also observed in the UV with the Wide Field Planetary Camera 2 (WFPC2), the Faint Object Camera (FOC) and the Space Telescope Imaging Spectrograph (STIS) aboard the Hubble Space Telescope. The UV emission are caused by excitation of H_2 by impinging electrons. STIS images are shown on Figure 1 and on Figure 10. Figure 10 also shows the discovery of footprint auroral emissions related to other Galilean satellites: Europa and Ganymede.

Since 1993, hundreds of Io flux tube footprint observations have been accumulated both in the IR and UV and they are very similar (Connerney et al, 1993, Clarke et al., 1996, 1998, Prange et al., 1998). They show in both hemispheres:

- A spot (hereafter called the "**Io spot**") that follows, with some longitudinal shift, Io's instantaneous location on its orbit. The size of this spot seems to be variable, sometimes as small as 200 km (Prange et al, 1996), sometimes as extended as 2000 km (Clarke et al, 1996). As a comparison, the magnetic projection of Io's diameter, on the Jovian ionosphere is ~150 km (Clarke, personal communication). It would not be surprising that the Io spot emissions were actually composed of many very thin structures like the discrete auroral arcs on Earth (<100 m) (Otto and Birk, 1993). The HST cameras are not able to resolve any thin structure that might exist in the Io spot/tail emissions: the latitudinal size of the Io spot itself is comparable to the size of the point-spread function of the cameras (the latitudinal size of the Io spot ~500-2,000km and the STIS resolution ~1,000km in ~15 pixels)

- A long **trailing tail** (> 90^o of longitude) follows the Io spot and becomes dimmer further from the spot. On some images, the tail is not continuous but divided in distinct spots. Figure 11 shows an IR image of the trailing tail in the northern hemisphere, divided in 5 distinct spots separated by ~5^o. A simultaneous observation of the southern hemisphere shows 2 distinct spots separated by ~4^o. Some UV images show multi-spot features as well. STIS images taken in 1998 detected two spots in the northern hemisphere separated by 3,800km (~6^o) and in 1999, 2 spots separated by 1,800km (~3^o) (Clarke et al., AGU 2000, unpublished data, personal communication). As stated by Connerney, the distinct spots are small and difficult to resolve and it may well be that the tail always displays a multi-spot pattern. This pattern may have been observed in the last two years simply because of improvements of the technique of IR observation (Connerney and Satoh, 2000). On the other hand, it seems to me that the UV observations technique have not changed that much. For instance, one of the most recent STIS images of Jupiter, taken on December 2000 shows a tail that is now once again continuous. The exposure time was short enough (2 minutes) to avoid a possible blurring of distinct spots by the fast Jupiter's rotation (blurring is ~1^o per minute). It is probable that the nature of the Io interaction changes in time in response to change of the density of the plasma torus. In 1998-1999, Galileo measured a plasma density in the warm torus that was twice the density measured

by Voyager (see section 2.2). Both IR and UV multi-spot observations were obtained during this period and, at the time of the observation, Io was in the center of the wobbling torus.

Figure 10: UV image of the aurora and the Io spot and its trailing tail.

Also shown, at the center of the image, are emissions of the footprint of Ganymede (center just below the oval) and Europa (to the right of Ganymede'spot). (http://www.sprl.umich.edu/cassinihstjupiterflyby)

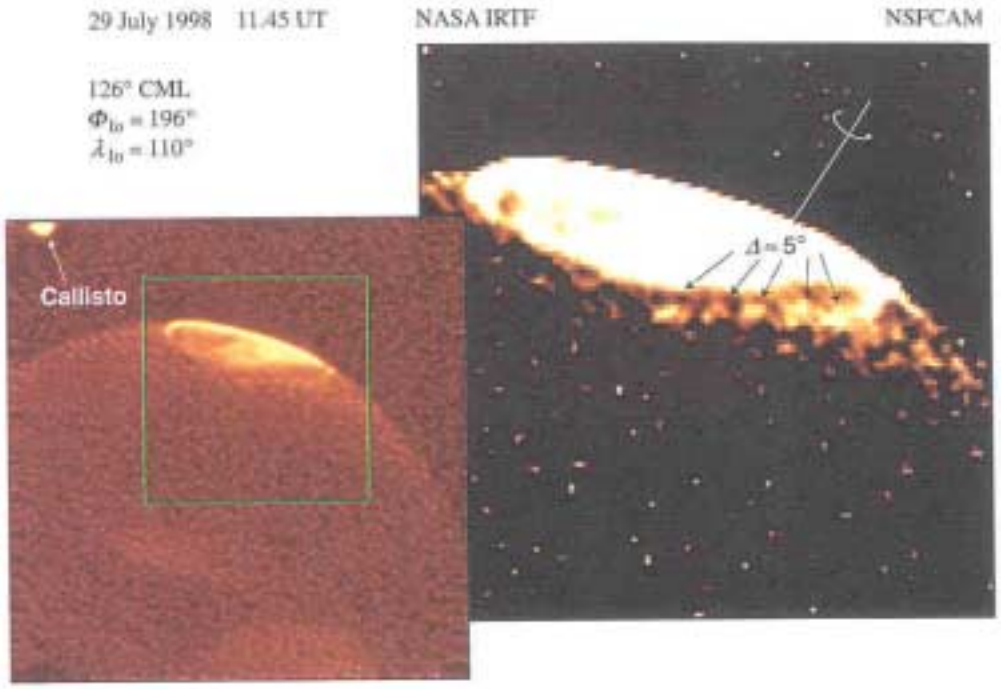

Figure 11: IR observation of the trailing tail divided in multiple spots.
(From Connerney and Satoh, 2000)

All IR and UV observers tried to measure what they call the *lead-angle* of the Io spot relative to the instantaneous location of Io projected on Jupiter. We think that this *lead-angle* concept is sometimes ambiguous. Let's think in the frame of the open-loop Alfven wing model. In section 3.2, we used the term *lead-angle* as the angle between the instantaneous location of Io projected on Jupiter' surface and the foot of the Alfven wing. But is it the same angle as the angle between this instantaneous location of Io and the *observed* Io spot? This would be true only if the acceleration process takes place close to the foot of the Alfven wing. But if the acceleration process takes place somewhere along the Alfven wing far from the Jupiter' ionosphere, then this *observed angle* should be smaller than the *lead-angle*. As none of the models include explicitly an acceleration mechanism, we think that the two concepts are a source of confusion in the published articles about the observation of the Io spot (Connerney et al. (1993), Prange et al. (1996), Clarke et al. (1998)). We will thus use the term ***observed shift angle*** for the observed angle between the instantaneous *Io's location* and *Io spot* and keep the term ***lead-angle*** for the angle between the *foot of the Alfven wing* and *Io's instantaneous location*. In the section dedicated to numerical

modeling with a 3D code (section 4.3) of the acceleration process, the difference between the two concepts will be clearly noticeable and will be recalled. Anyway, the computations of the *observed shift angle* were limited because of the inaccuracy (~10^o) of the GSFCO6 magnetic field model used for the mapping of the instantaneous location of Io. This uncertainty is almost as large as the *observed shift angle* itself. In the literature, it is usually claimed that a large *observed shift angle* would favor a unipolar inductor model while a small angle would favor the Alfven wave model. It should be noted that this is true despite the confused definition of this angle. The unipolar inductor *lead-angle* will always be larger than the open-loop *lead-angle*. Connerney et al. (1993) measured in the IR images, an *observed shift angle* between 15^o and 20^o and claimed that it favored the unipolar inductor Model. Clarke et al. (1996, 1998) and Prange et al. (1996, 1998), using GSFCO6 and VIP4 models reported an *observed shift angle* between 0 and 15^0, which do not seem to confirm any of the two standard models.

Another interesting point of the IR and UV image analysis is the measurement of the Io spot brightness. Prange et al. (1996) measured the total power radiated in the H_2 UV-emission bands over the Io spot. Using a model of energy degradation, they estimate the power input precipitation in the Io spot ~2-3 x 10^{11} W. They claimed that this remarkably high figure represents ¼ of the total system energy provided by the motion of Io across Jovian magnetic field lines (estimated as ~10^{12} W per hemisphere for a 3 10^6 amp Voyager1-current and a 400 kV potential across Io's diameter). Clarke et al. (1996) and Prange et al. (1998) confirmed these numbers. They concluded that most of the energy of the Alfven wave is deposited in the first interaction with the Jovian ionosphere and Prange et al. (1996) stated that it was not a surprise to observe only a single spot, which proved to be not always the case in the 1998-1999 observations.

Because of the tilted and asymmetric Jovian magnetic field, the torus moves north and south with respect to Io, thereby varying the column of plasma that an Ionian Alfven wave would experience on its way to Jupiter's ionosphere. Moreover, because of this wobbling of the magnetosphere at Io, the field strength varies by ~20 %. It might be expected that these geometrical variations will have an effect on the *observed shift angle* and on the brightness of the Io spot. Prange et al. (1998) and Clarke et al. (1996) showed that the south and north shift angles are indeed anti-correlated. The north shift angle is close to zero when Io is above the torus (Io's sub-longitude in the S_{III} system =180^o) while the south shift angle is maximum. The opposite is observed when Io is under the torus (S_{III} ~0-50^o). These observations fit well with the picture of

an Alfven wave traveling through the torus. Clarke et al. (1998) searched for a correlation between the brightness of the Io spot and the sub-Io longitude but couldn't find any clear trends.

3.3.4. Io spot spectroscopy

Finally, some more pieces of information were obtained through the UV spectroscopic analysis of the Io spot using the Goddard High Resolution Spectrometer (GHRS) aboard the HST. The Io spot spectra are consistent with emission of the H_2 molecule excited by electron impacts. The GHRS spectra isolated the Werner and Lyman bands of the H_2 emissions (between 900 Å and 1800 Å). When the observed spectra are compared to laboratory spectra of H_2 excited by an electron beam, it is clear that the Werner part of the observed spectra is too dim compared to the Lyman part. This is interpreted as absorption by methane, a minor constituent of the Jupiter's atmosphere. The methane UV absorption cross section is maximum over the Werner band and decreases rapidly at 1300 Å over the Lyman band. Using a model of the Jovian atmosphere, one can deduce the altitude of the deposition of energy of the impinging particles and, using a model of degradation of energy, deduce the energy of the primary particles at the top of the Jovian atmosphere. Assuming that the primary particles are electrons with a maxwellian distribution, Dols et al. (2000) computed an energy ~ 60 KeV for the impinging electrons, similar to the energy deduced from the main auroral oval spectra. The assumption of electrons as primary particles is still an issue but if sulfur or oxygen ions were the primary impinging particles, their energy at the top of the Jupiter atmosphere should be about >1 MeV to produce the same spectrum at the same altitude (Grodent, personal communication). As stated in section 2.2, the electrons or heavy ions in the torus are not that energetic thus an acceleration mechanism seems to be at work along the Io flux tube.

3. 4. What can be concluded from the observations?

The observations discussed in the former section are difficult to interpret in one or the other model. Moreover, these models don't include explicitly any process to accelerate particles and precipitate them in the Jovian ionosphere. Crary and Bagenal (1997) proposed a hybrid model that addresses both issues. His idea is based on the Galileo measurements of the plasma flow close to Io. Galileo flew within 1.4 R_{Io}, ahead of the satellite, downstream with respect to the

corotating plasma flow, close to Io's equatorial plane. The flow measured in this wake was quasi-stagnant, with speed less than 1 km/s (Bagenal, 1997). Crary interprets this flow as typical of the flow around Io. Because of this slow flow, Crary claims that the Alfven wave would have plenty of time to bounce back exactly at Io and evolve in the steady state current loop described by the Unipolar model. His idea is a two-step interaction: the interaction would start as an Open–loop Alfven model. He proposes that the finite electron inertia on this Alfven wave, which was not considered in any previous discussion, produces a parallel electric field that would accelerate electrons to create the Io spot emissions (Crary, 1997). Because of the slow flow close to Io, the system would evolve into a steady current loop that would explain the DAM modulation by Io and the faint trailing tail extending away from the Io spot. As stated by Crary et al. (1997), the treatment of the wave-particle interaction in this study is limited and further quantitative modeling might make his point convincing.

Besides this modeling issue, the data themselves are sometimes contradictory and it doesn't seem to be due to improper data analysis. It seems that the interaction of Io and the magnetized plasma is intrinsically variable: the size of the Io spot is variable, the tail is sometimes continuous, sometimes divided in distinct spots, the power dissipated in the Io spot is sometimes close to the maximum available energy but at other times, the multi-spot observations shows that the energy cannot be completely lost at the first interaction with the ionosphere. The *observed shift angle* seems to vary between 0 and 15^{o}.

Connerney and Satoh (2000), following Neubauer (1981), propose that the Io interaction changes in time from the Unipolar model to the Open-loop Alfven Wave model depending on Io's longitude. They stated that what is lacking now is a theory that encompasses the variable behavior of the Io/Jupiter interaction. The sources of variability in the system are multiple: the torus density, the structure of the torus (as illustrated by the disappearance of the ribbon in the Galileo measurements), Io's location in the torus, Io's orbital longitude, the Jovian ionosphere conductivity, the neutral density around Io, etc. Some of these parameters could, in principle, be studied with a proper quantitative model of the Io/Jupiter interaction. In this thesis, we try to work with these issues in mind: the acceleration mechanisms proposed in the next chapter is the formation of a localized parallel electric field associated with localized anomalous resistivity triggered by the current along the Alfven wing. This parallel electric field leads to a reconfiguration of the field line topology, or reconnection. The variability of Io's location relative to the torus, of Jupiter's conductivity and of the torus plasma density will affect the Alfven wave

propagation and thus the location of the acceleration process. These issues will be addressed in chapter 5 as part of the simulations results.

CHAPTER 4: "RESISTIVE RECONNECTION " MECHANISM: FORMATION OF A LOCALIZED ACCELERATING PARALLEL ELECTRIC FIELD

4. 1. Why study specifically resistive reconnection?

As stated before, the Io spot auroral emission, and the deduced precipitating particle energy are evidence of the existence of an acceleration mechanism somewhere along the field lines connecting Io to the Jovian ionosphere.

The mechanism that we consider (resistive reconnection) creates a localized parallel electric field that would precipitate particles down to the Jovian ionosphere. It will be shown in the next section that the key idea of the "resistive reconnection" mechanism is that the onset of the parallel electric field depends on the magnitude of the parallel current. This means that we will consider a simplified version of Ohm's law, limited to the resistive current term: $\boldsymbol{E}_{//} = \eta \boldsymbol{J}_{//}$ where $\boldsymbol{E}_{//}$ is the electric field parallel to the Jovian field lines, $\boldsymbol{J}_{//}$ the current parallel to the Jovian field lines and η the electric resistivity. In principle, a parallel current is not the only way to create a parallel electric field: any term in Ohm's law that has a component parallel to the background Jovian magnetic field might create a parallel electric field (the electron pressure gradient etc.). So the question is: Why is it appealing to consider a current-generated, parallel electric field?

The first part of the answer is the structure of the Io-related, auroral emissions: They do not appear uniformly along the footprint of the whole torus. They are localized in the vicinity of Io's sub-longitude, which means that the acceleration mechanism is related to the localized perturbation that Io creates in the magnetosphere. The second part of the answer is that most of the perturbation can be described as the propagation of an Alfven wave along the Io flux tube. It will be shown in the next section that the magnetic component of the Alfven wave induces a parallel current flowing along the Io flux tube. To sum up, we can say that the auroral emission is clearly related to the Io's perturbation and that this localized perturbation is equivalent to a

current flowing along the Io flux tube. **Consequently, in our mechanism, the onset of the localized parallel electric field depends on the magnitude of the parallel current**. This onset depends also on the existence of resistivity somewhere along the field line. Where does this resistivity come from? Close to Io, the collisions between neutrals and electrons can provide the usual collisional resistivity but further down the field lines, the plasma density becomes small and the binary collisions might be too rare. In this case, anomalous resistivity can be provided by excitation of some micro-instabilities triggered by the plasma condition along the field line (see chapter 6). Let's state clearly that, because of the limited resolution and the limited physical processes that we consider in our numerical code, we won't try to model this resistivity. We will make the **a priori assumption** that some resistivity exists along the field line: If the current density rises up to a prescribed critical value, then some micro-instabilities can be excited and lead to anomalous resistivity.

The resistive current approach is even more general than it looks. As stated before, there are plenty of other ways to form a parallel electric field on many different scales, simply by looking at all the terms in the Generalized Ohm's law beyond the resitive current term. All the terms in the Generalized Ohm's law, beside the resistive term, imply other physics at other (smaller) length scales. But if these terms play a role in a microscopic reconnection process, we can reasonably imagine that at a larger scale, their effect may be parameterized by the most significant perturbation present in the Io/torus system: the parallel current. This means that the resistivity that we will be using in the modeling is actually more than a regular resistivity: it should be understood as a parameterization of the average of all the processes that can create a parallel electric field at smaller length scales.

Another appealing aspect of the "resistive reconnection" mechanism proposed here is that it considers the Io/torus interaction in a self-consistent way. Usually, most theories of auroral acceleration are local, i.e., they don't consider the implication of the formation of a parallel electric field on the structure of the background field itself. The parallel electric field changes the topology of the background magnetic field lines (reconnection of some field lines) and consequently will have an effect on the formation of the electric field itself. This issue can be addressed self-consistently by the 3D resistive MHD modeling.

In this chapter, we first recall the basic concepts of the resistive reconnection process applied to the Io/Jupiter interaction. Next, we show the results of a 3D numerical simulation of this

interaction that includes the reconnection process in the self-consistent way described in the former paragraph. These results illustrate the potential of resistive reconnection as a particle acceleration process. They show that the model reproduces nicely some observed features of the Io/torus interaction, like the plasma wake downstream of Io and the extended trailing tail in the Jupiter's ionosphere. The model used is a full 3D MHD code including plasma and neutrals that is adapted to the Io/Jupiter situation (Birk and Otto, 1995). Some simplifications were made to run these simulations: the plasma density and the Jovian magnetic field are assumed to be uniform. The results are thus limited to these simplifications. The inclusion of a realistic description of the magnetosphere in the 3D MHD code is beyond the scope of this thesis. The effect of a realistic description of the Jupiter's magnetic field and the torus density profile will be investigated in the next chapters with a simpler model.

4. 2. "Resistive reconnection" mechanism

The Io/torus interaction is sketched on Figure 12. We assume Io moves relative to the dense plasma torus at a velocity $\mathbf{V}_{Io}$=57 km/s. The plasma of the torus sweeps the neutrals of Io's atmosphere. These collisions lead to the ionization of some of the neutrals and to the slowing down of the torus plasma by friction. The ionization and friction are the sources of a magnetic perturbation ($\boldsymbol{B}_{\perp}$ in blue on Fig.12 b) perpendicular to the Jovian magnetic field ($\mathbf{B}_0$) that propagates as an Alfven wave with velocity V_A along the field lines connecting Io and Jupiter (Fig. 12 a, b, c). On the flanks of Io, the field lines are just dragged in the plasma torus, unperturbed (sketched as a red field line).

A field-aligned current (in blue on Fig. 12 a, c) flows between the perturbed (black) and the unperturbed (red) field lines consistently with Ampere's law.

$$\boldsymbol{J}_{//} = -\nabla \mathrm{x}\, \boldsymbol{B}_{\perp}$$

If we assume that there is some localized resistivity η somewhere in this current sheet (hatched green zone), then, following Ohm's law (in a simplified version), a parallel electric field should exist through this region.

$$\boldsymbol{E}_{//} = \eta \boldsymbol{J}_{//}$$

This parallel electric field accelerates particles along the field line and drives the change of the magnetic field topology as shown by Faraday's law.

$$\frac{\partial B_{\perp}}{\partial t} = -\nabla \mathrm{x} \boldsymbol{E}_{/\!/}$$

The magnetic perturbation $\boldsymbol{B}_{\perp}$ generates a new magnetic connection of field lines perturbed by Io's Alfven wave and the unperturbed magnetic field as illustrated in Fig. 12 d.

This is basically the physics that is modeled in the 3D MHD code described in the next section.

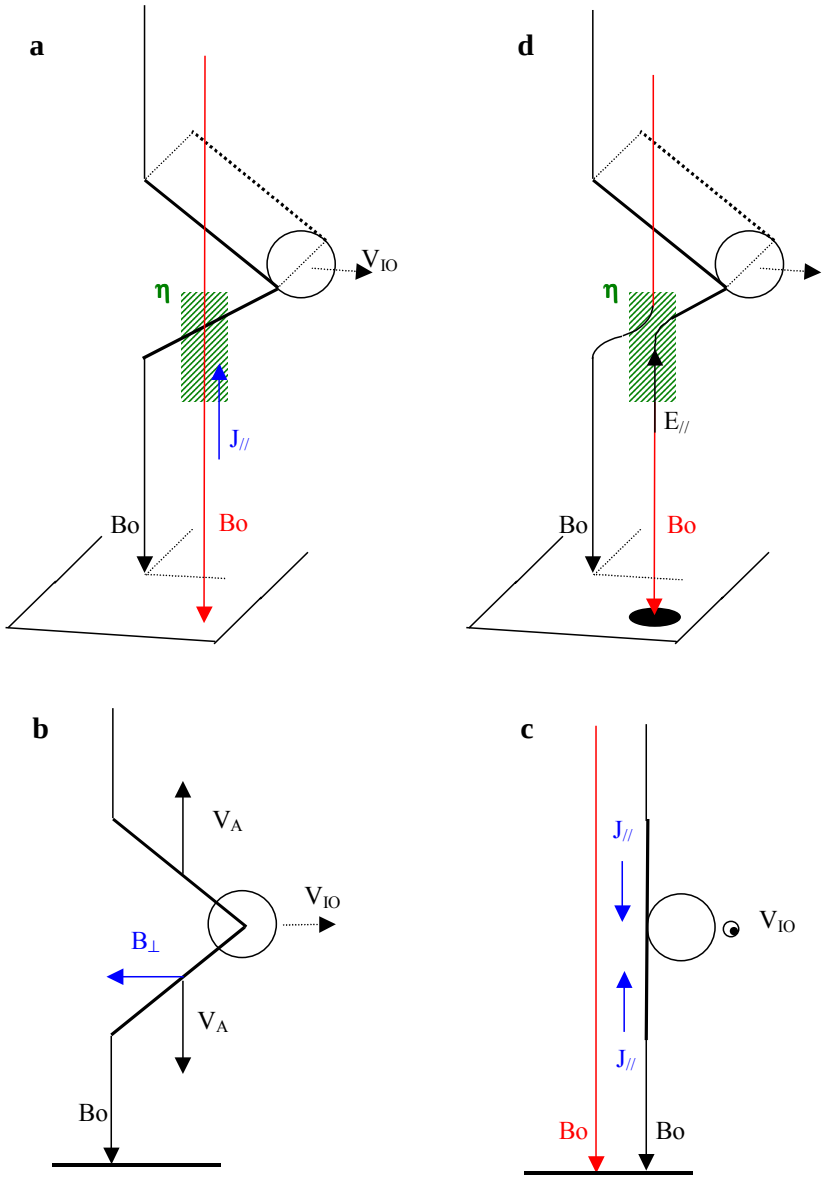

Figure 12: Sketch of the Io/torus interaction.

Fig.a *shows the Alfvenic magnetic perturbation created by Io's motion, propagating down the magnetic field line crossing Io's orbit (in black) toward the Jovian ionosphere (at the bottom of each sketch). On the flanks of Io, the red field line is unperturbed. The hatched green zone represents a zone of localized resistivity η.* ***Fig.b*** *is a side view of Fig.a, emphasizing the* $\boldsymbol{B}_\perp$ *magnetic component of the Alfven wave (in blue).* ***Fig.c*** *is a front view of Fig.a showing the current* $J_{//}$ *flowing between the unperturbed field lines and the field line perturbed by Io.* ***Fig.d*** *shows the change of the field line topology caused by the parallel electric field and the ionospheric auroral emission at the end of the reconnected field line (black spot). These sketches illustrate magnetic reconnection close to Io but the process can be anywhere along the field line provided that some resistivity is available.*

4. 3. 3D MHD illustration of the reconnection process

4.3.1. Simulation geometry

The simulation geometry at the beginning of the simulation is illustrated on Figure 13 as follows.

- To simplify the computation, a rectangular coordinate system is used: the Jupiter field lines are unbent and represented by vertical straight lines along the Z-axis. To save computational resources, the size of the simulation box is small: the distance between Io and Jupiter (along the Z-axis) is limited to 50 R_{Io} (the real length is about 280 R_{Io}), the Y size = 40 R_{Io} and the X size = 5 R_{Io}.

- The Jovian ionosphere is at the bottom of the box in the XY plane at Z=0 and one half of the Io's neutral cloud is represented at the top at Z=50. Io is not represented as a hard body with an atmosphere, but merely a cloud of neutrals, about the size of Io itself. We assume that this cloud is an infinite reservoir of neutrals and maintain the ionization rate consistent with the observations of Bagenal (1997).

- The simulation is run in the reference frame of the torus: the plasma torus and Jovian magnetic field are still and Io is moving in this background plasma from left to right along the Y-axis. To save computational resources, periodical boundary conditions are used at the Y boundaries. When Io exits the box on the right, it comes back in the simulation box on the left.

4.3.2. Simplified magnetosphere description

We assume that the magnetic field of Jupiter is not changing along the field line: the field is uniform and that the torus plasma density is not varying along the field line. The background plasma density is uniform as if the torus extended uniformly from Io's orbit to Jupiter's ionosphere.

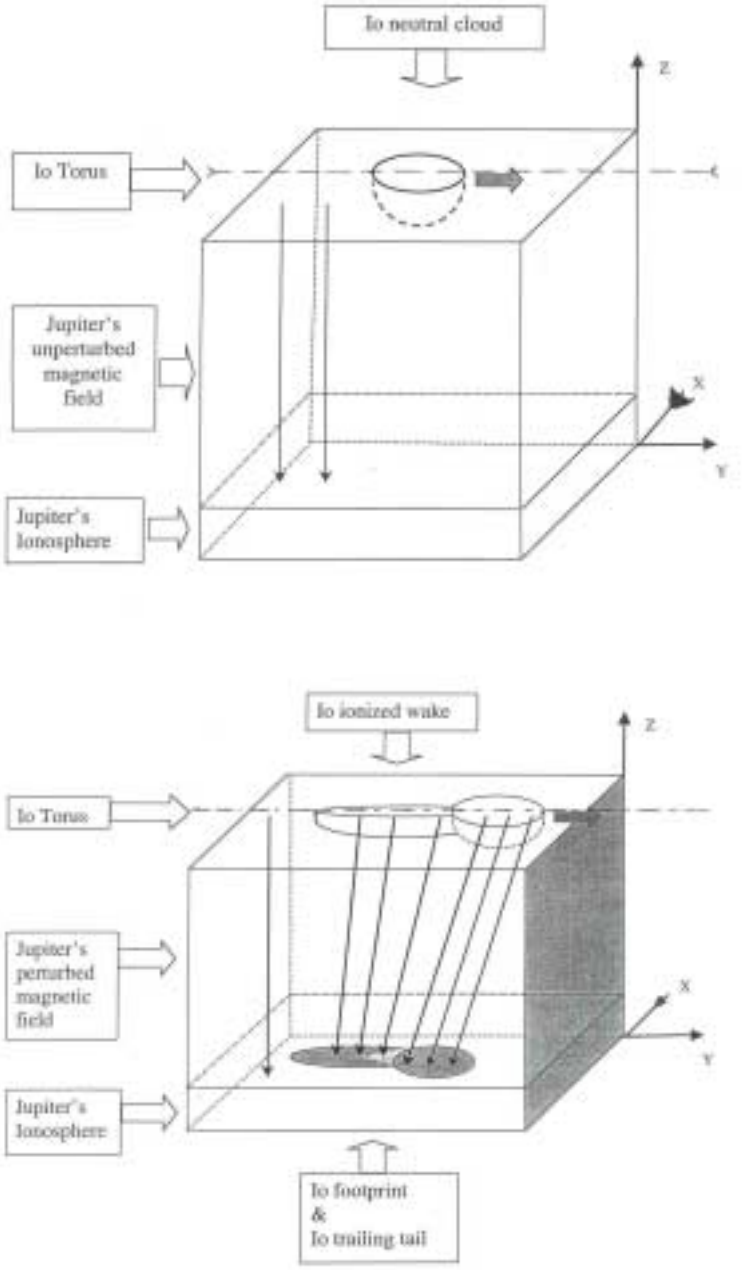

Figure 13: Geometry of the 3D simulations.

The top panel shows the initial condition at time =0 and the bottom panel shows the Io/Jupiter interaction in the course of the simulation.

4.3.3. MHD equations

The following equations of resistive MHD are written in their normalized form (see next section). They are solved with a finite-difference Leapfrog scheme, which is second-order accurate in space and time.

1. The plasma continuity equation includes an ionization term:

$$\frac{\partial \rho}{\partial t} = -\nabla . \rho \, \boldsymbol{u} + \rho \mu_c$$

μ_c : The specific ionization rate

2. The plasma momentum equation includes an ionization term, a "torus" friction term (between plasma and Io's neutral) and an "ionosphere" friction term (between plasma and neutrals in the ionosphere of Jupiter)

$$\frac{\partial \rho \, \boldsymbol{u}}{\partial t} = -\nabla . \rho \, \boldsymbol{u} \, \boldsymbol{u} - \frac{1}{2} \nabla p + \boldsymbol{J} \times \boldsymbol{B} + \mu_c \rho \, \boldsymbol{u} - \nu_{in} \rho \, (\boldsymbol{u} - \boldsymbol{u_{io}}) \; - \nu_{in} \rho \, \boldsymbol{u}$$

$\nu_{in} \rho \, (\boldsymbol{u} - \boldsymbol{u_{io}})$: Friction term in Io's cloud

$\nu_{in} \rho \, \boldsymbol{u}$: Friction term in Jupiter's ionosphere

B : The total magnetic field including the Jovian magnetic field $\mathbf{B_0}$ and the magnetic perturbation created by the Alfven wave.

3. The plasma pressure equation is the adiabatic equation and includes the friction and ionization terms:

$$\frac{3}{2} \frac{\partial p}{\partial t} = -\frac{3}{2} \nabla . p \, \boldsymbol{u} + p \nabla . \boldsymbol{u} + Q$$

Q: source of energy including Joule heating, heating by friction and ionization and loss by cooling of the plasma by Io's cold neutrals.

4. The set of equation is closed using the law of ideal gas:

$$p = \rho k T$$

5. Ampere and Faraday's laws are used in their MHD approximation:

$$\nabla \mathrm{x} \boldsymbol{B} = \boldsymbol{J}$$

$$\frac{\partial \boldsymbol{B}}{\partial t} = -\nabla \mathrm{x} \boldsymbol{E}$$

6. Ohm's law includes a resistive term:

$$\boldsymbol{E} = -\boldsymbol{u} \times \boldsymbol{B} + \eta \boldsymbol{J}$$

The resistivity is prescribed and switched on when the current rises up to a fixed critical current (J_c). This parameterization is common and simply means that the field-aligned current cannot increase indefinitely because some instability will be excited and will limit the current, acting as an increased resistivity.

$$\eta = \eta_0 (J - J_c) H(J - J_c)$$

$$H(J - J_c) = 1 \quad \text{If } x > 0$$

$$= 0 \quad \text{If } x \leq 0$$

4.3.4. Numerical parameters and normalization

- In the continuity and momentum equations, we need the effective ionization rate μ_c: the number of ions produced per second. This number is deduced from spacecraft measurements. Galileo, when crossing the Io's wake, measured the total ionization rate in Io's vicinity I= 5 x 10^{27} sec^{-1} (Bagenal, 1997). The effective ionization rate is the total ionization rate divided by the number of plasma particles taking part to the ionization in the Io's cloud. Assuming an ionization volume the size of Io itself and a torus ion density ~2000 1/cm3, we get an effective ionization rate ~0.1 sec^{-1}. This is probably too low as the total ionization rate deduced from Voyager 1 was six times larger than the one computed by Bagenal, but this estimate is good enough to get reasonable results from the simulations.

- The elastic ion/neutral collision rate is not known. In this work, the collision frequency is assumed to be equal to the ionization frequency, which means that we don't favor any process as both contribute equally to the momentum term.

- All quantities have been made dimensionless by normalization to typical figures close to Io. The physical units are obtained by multiplying the normalized units appearing in the figures showing the results by these normalization factors.

The plasma mass density ρ is normalized to the plasma density in the middle of the torus:

ρ_0= 53,000 amu/cm^3

The characteristic length is normalized to the Io's radius: **L_0= 1,820 km**

The magnetic field component is normalized to the Jupiter's magnetic field strength at the Io's orbit: **B_0 ~2,000 nT.**

The other normalization factors are deduced from the former ones:

The velocity of the plasma and Io's relative velocity are normalized to the Alfven velocity in the center of the torus: **$V_0 = B_0 / (\mu_0 \times \rho_0)^{1/2}$ ~200km/s**.

The time scale is normalized to **$T_0 = L_0/V_0$ ~ 10 sec**

The electric field is normalized to **$E_0 = B_0 \times L_0 / T_0$ ~0.4 V/m**

The electric potential to **$\Phi_0 = E_0 L_0$ ~650 kV**

The current density to **$J_0 = B_0/L_0$ ~4 x 10^{-6} A/m^2**

The critical current **J_c= 0.05 J_0** and **η_0= 0.1**. These figures are arbitrary and were changed as part of sensitivity experiments that are not shown here.

4.3.5. Results of the simulations

1. Wake formation

Figure 14 shows the formation of a wake of freshly ionized plasma on the Io's orbit, downstream of Io. The view is in a horizontal plane, parallel to the X-Y plane of Figure 13 , at the altitude of Io's orbit at Z=50 R_{Io}. Io is moving up along the Y-axis. Only one half of Io is shown here, the center of Io is thus moving on the Y-axis itself.

- During the time of the simulation (time= 40 T_0), Io has moved from Y=0 to Y=15.

- On the left panel, the color scale shows the plasma density. It is maximum at the center of Io where most of the ionization takes place and extends in a long high-density wake downstream of Io.
- The right panel shows the pressure. In the wake, the pressure is low and the density is high compared to the background torus plasma.

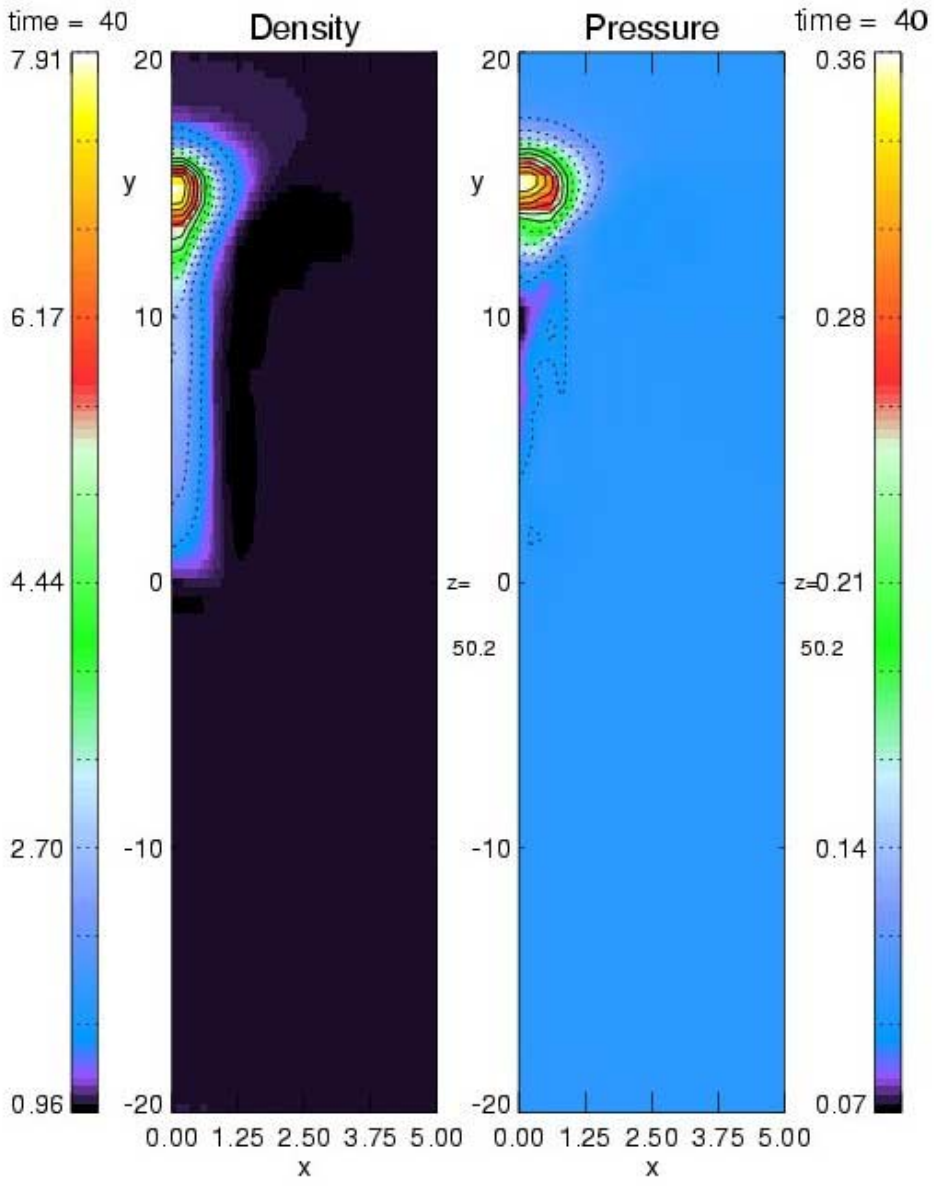

Figure 14: 3D simulation: Formation of a wake behind Io.

2. Propagation of the Alfven wing

Figure 15 shows, from upper left to lower right, 4 snapshots (time=20, 40, 60, 90 T_0) of the propagation of the Alfven wave magnetic perturbation generated by the motion of the neutral cloud. The view is in the Y-Z plane of: The Jovian ionosphere is at the bottom, half of Io's cloud is at the top moving from left to right.

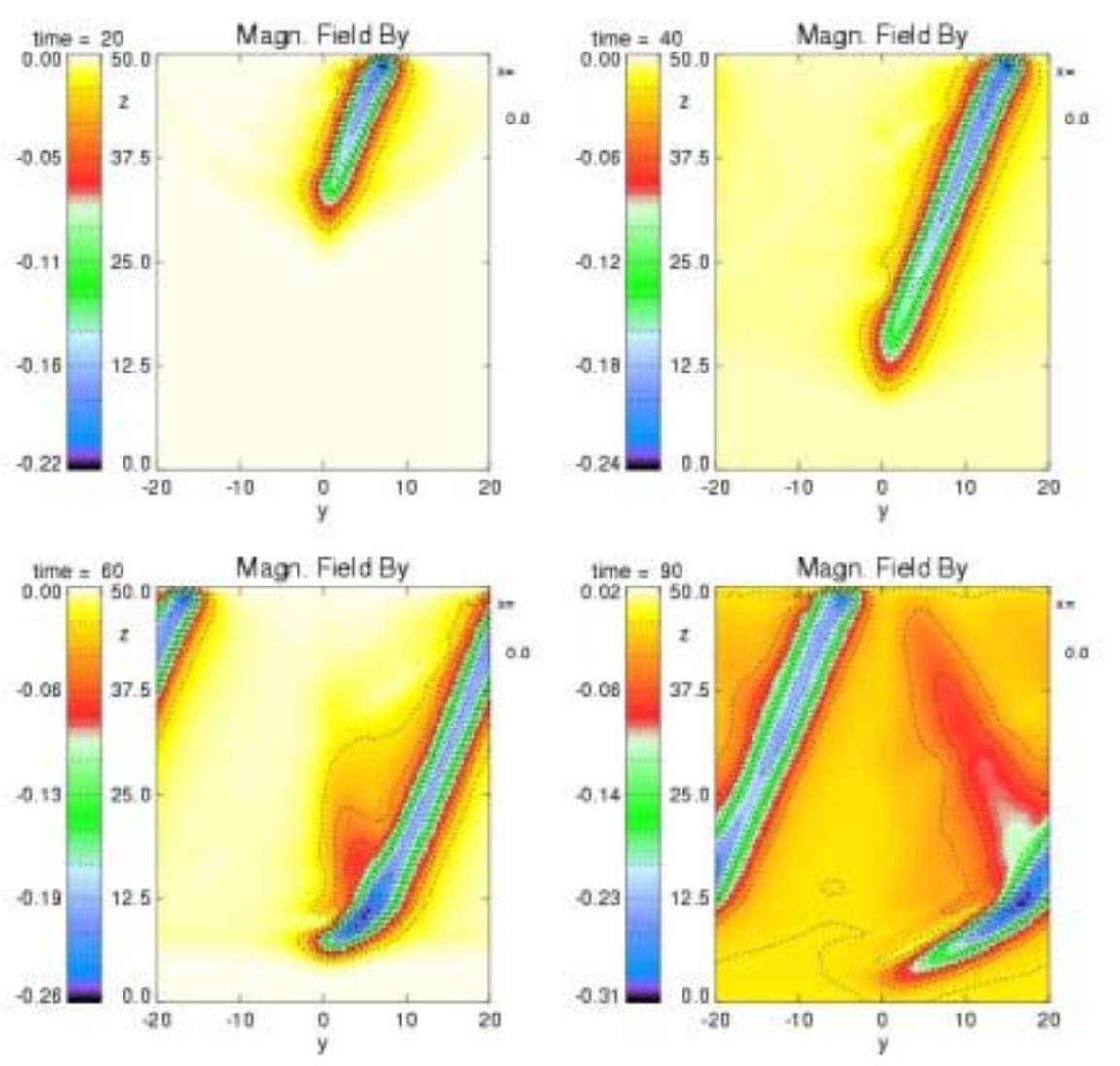

Figure 15: 3D simulation: Propagation of the Alfven Wing.

The color scale illustrates the magnitude of the Alfven wave magnetic perturbation $\boldsymbol{B}_{\perp}$ (in the coordinate frame used here, $\boldsymbol{B}_{\perp}$=By). The magnetic perturbations propagating on different field lines form the so-called " Alfven Wing". Because of the assumption of uniform background field and torus plasma density, the magnitude of $\boldsymbol{B}_{\perp}$ is almost constant along the wing, from Io to the Jovian ionosphere. The slight decrease is caused by reconnection taking place along this wing and will be illustrated in the following plots.

- The angle of the Alfven wing relative to the Jovian magnetic field (The Mach angle θ) is determined by Io's relative velocity and the Alfven velocity tan (θ)= V_{Io} / V_A. Because of the assumption of uniform background field and plasma density, the Alfven velocity is constant over the simulation box and the Mach angle is constant along the Alfven wing. Thus the *lead-angle* (at the footprint of the Alfven wing) is equal to the Mach angle. In the Io's frame of reference, the torus plasma would move from right to left and the wing would Io or, in other words, be located downstream of Io.

- The lower left panels illustrate the reflection of the Alfven wave on the Jupiter's ionosphere. Because of the periodic boundary conditions Io is leaving the box on the right and re-entering it on the left.

The following figures show a horizontal cut through the wing at the time = 40 T_0 (right upper panel of Figure 15 at mid-distance between Io and the ionosphere (Z ~33 R_{Io})). The view plane is parallel to the X-Y plane of Figure 13. Io is moving up along the Y-axis. Only one half of Io is shown here, the center of Io is thus moving on the Y-axis itself.

3. Alfven magnetic component

Figure 16 illustrates better the horizontal magnetic perturbation in the Alfven wing. The color scale in the 2 panels shows the magnitude of the Jovian background magnetic field (B_0=B_z here), unperturbed far from the wing, slightly decreased in the wing itself. On the left panel, small arrows are superimposed in the horizontal plane. They represent the B_x and B_y components of the magnetic perturbation $\boldsymbol{B}_{\perp}$. The perturbation is larger close to the center of the wing and

decreases away from it. This is this perturbation that will reconnect if the local resistivity is switched on by the vertical current shown on the next figure.

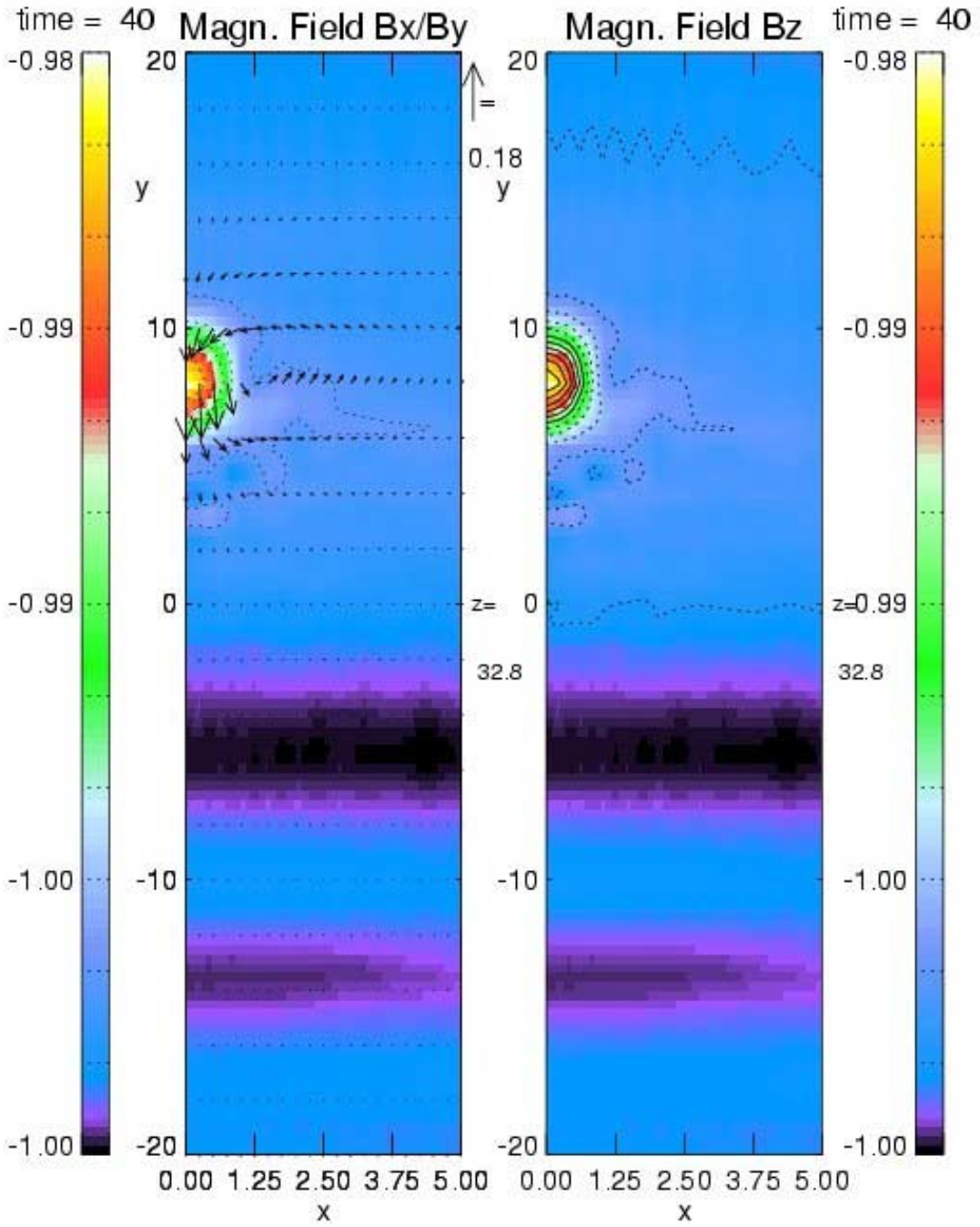

Figure 16: 3D simulation: The Alfven wave magnetic perturbation. Horizontal cut through the Alfven wing.

4. Parallel current

Figure 17 shows the field-aligned current that follows the magnetic perturbation shown on the former figure.

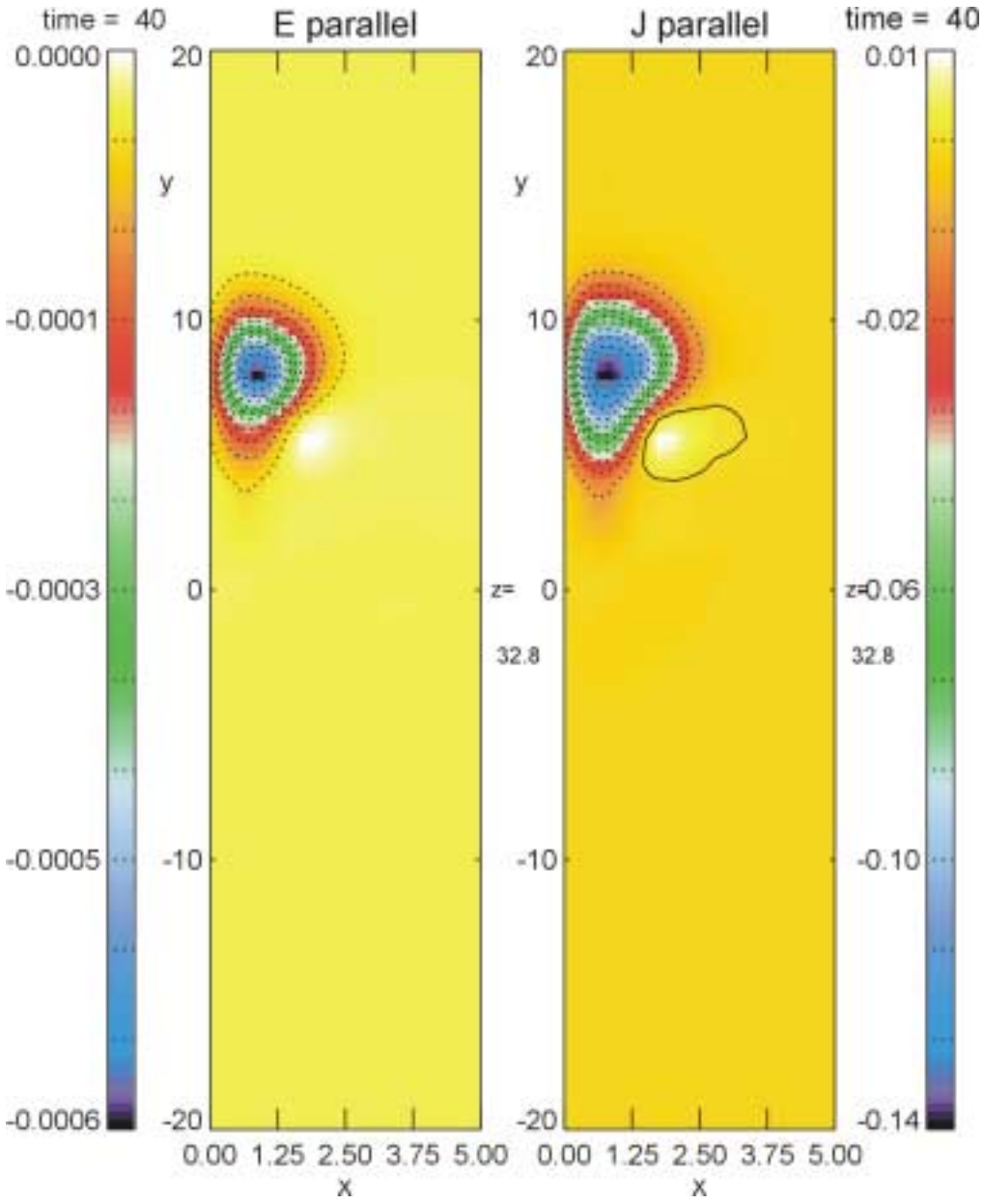

Figure 17: 3D simulation: The field-aligned current.
Horizontal cut through the Alfven wing.

On the right panel, the color plate indicates the magnitude of the field-aligned current created by the magnetic perturbation. It is maximum close to the edges of Io at a distance is about 1 R_{Io}. When this current rises up to the prescribed critical current, anomalous resistivity is switch on. On the left panel, the color plate shows the magnitude of the parallel electric field resulting from the switch-on of the resistivity by the parallel current. This is this electric field that could accelerate particles along the Jovian field lines, precipitate them in the Jupiter's ionosphere and lead to auroral emission close to the Io footprint.

5. Electric potential drop

Figure 18 shows, at time= $40T_0$, the potential drop that a particle will experience when the parallel electric field precipitate it along the field line in the Jovian ionosphere. An integration of the parallel electric field shown on the previous figure was performed along the field line, from the ionosphere to Io.

- This is a view in the X-Y horizontal plane at the bottom of the box. Io is moving up along the Y-axis. Only one half of Io is show here.

- The color scale shows the magnitude of this potential drop. Its maximum follows Io on its orbit, is located on the edges of Io ($\sim 1R_{Io}$) and decreases along a long tail, downstream of Io. Particles would be highly accelerated just under Io, at a longitude = the Io's sub-longitude and less accelerated downstream of Io. The resulting auroral emission, assuming a constant flux of particles, would be brighter close to the Io spot and dimmer further down a long trailing tail. This is highly reminiscent to the HST observations.

- In this simulation, the long trailing tail of the potential drop is caused by reconnection all along the Alfven wing. In these simulations, the tail is not caused by any process in the wake of Io although Kopp (1996) showed that the ionization can create a corotational lag in the wake that lead to the development of a field aligned current system along the wake. The absence of this wake current system was not investigated here but might be caused by the choice of the critical current. The extension of the ionospheric tail depends on the integrated parallel electric field, which depends on the switch-on of resistivity, which depends on the strength of the field-aligned current. Eventually, the length of the tail depends on the prescribed value of the critical current J_c. A small critical current Jc is easily reached by the field-aligned current and a resistivity (and

thus a parallel electric field) is easily switch on all along the Alfven wing and –maybe- along the wake of Io. On the other hand, a choice of a large critical current J_c will limit the resistivity switch-on where the field-aligned current is the strongest, close to Io and the tail would then be short.

- These simulations show clearly the difference between what I called the *lead-angle* and the *observed shift angle* in section 3.3: On the bottom-left snapshot of Figure 15 that shows the Alfven wing reaching the ionosphere, the *lead-angle* ~ $\tan^{-1}(25\ R_{Io}/50\ R_{Io}) \sim 25^{o.}$ Keep in mind that this number cannot be compared to any theoretical *lead-angle* as the geometry and plasma densities are unrealistic here. But the *observed shift angle* as shown on Figure 18 is actually close to zero because the maximum reconnection occurs close to Io.

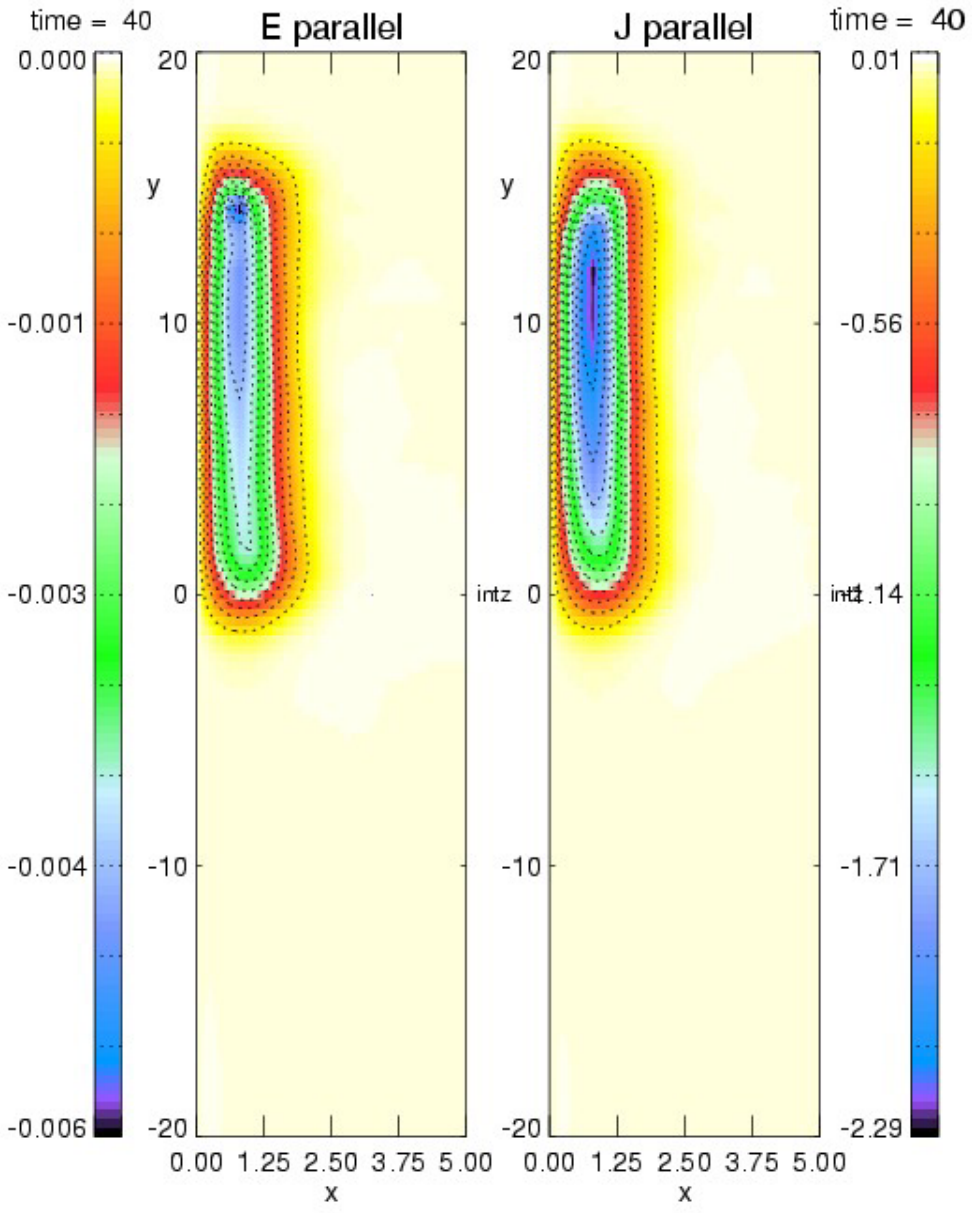

Figure 18: 3D simulation: The potential drop along field-lines.
This is interpreted as the structure of the auroral emissions on the Jovian ionosphere.

4. 4. Conclusions

1. The 3D MHD model used here includes all the basic physical processes we want to illustrate in this work. The sweeping torus plasma ionizes the Io neutral cloud and forms a long high-density wake behind Io. Friction and ionization slow down the torus plasma and create a magnetic perturbation that propagates toward the Jovian ionosphere as an Alfven wave. These Alfven wave perturbations form an Alfven wing. A current flows, bounding the Alfven wave, on the flanks of the wing. When this current rises above a critical current, anomalous resistivity is switched on, a local parallel electric field appears and the reconnection between adjacent field lines occurs. This electric field accelerates particles along the Jupiter field lines. These particles are precipitated in the Jovian ionosphere and produce auroral emissions in Jupiter's ionosphere in a spot following Io's location and in an extended tail trailing downstream of the Io spot. The main observed features of the Io/Jupiter interaction are thus nicely reproduced.

2. The structure of the Io spot and tail might, at first sight, be surprising. The Figure 18 showing horizontal views of the potential drop displays only one half of the simulation box. The maximum of the potential drop appears on the projected edges of the Io's cloud. One might then conclude that a similar pattern should be present on the left side of the Y-axis and that the observed Io auroral emissions should be structured in two parallel Io spots and trailing tails. Indeed, that is what the model would simulate. This two-structure pattern is a consequence of the low resolution of the model. At high resolution, the current sheets might be very thin with currents flowing up and down all across the Io flux tube. The reconnection would take place on a very small scale. Consequently, the Io's auroral emissions would be structured in very thin auroral filaments that would fill the entire Io's flux tube section. The current HST imaging cameras cannot resolve structures smaller than the Io spot itself.

3. The picture given by these results is that of a reconnection process that takes place all along the Alfven wing, but maximum reconnection occurs very close to Io where the parallel current is larger. These conclusions are limited to the simple assumptions of a constant Jupiter magnetic field and a uniform torus plasma density. A more realistic description of magnetosphere that would include the variation of Jupiter's field and plasma density along the field line crossing Io would definitely change the propagation of the Alfven waves. Where the field is high and plasma density low, the Alfven velocity is going to be large and the Alfven magnetic perturbation small.

Moreover, propagating in a density gradient, the Alfven wave will be partly reflected and partly transmitted on its way through the torus. In general, the Alfven wave propagation will be more complex and the reconnection location where the acceleration parallel electric field occurs might be different from the one given by the 3D illustration. The inclusion of the varying magnetic field and the torus plasma density profile in the 3D MHD code is beyond the scope of this work. We may learn as much physics by using a simpler 1D MHD model with a higher resolution. This 1D code is easier to handle and allows for some fast runs. That is the topic of the next chapters

CHAPTER 5: 1D SIMULATION OF THE ALFVEN WAVE PROPAGATION IN THE IO TORUS AND 2D MAPPING OF THE ALFVEN WING

5. 1. Motivation and potential of the 1D study

We use a 1D MHD model to study the Alfven wave propagation in a realistic magnetosphere description: The Jovian magnetic field and the torus density profile. The spatial dimension that we consider in the 1D modeling is the dimension along a field line connecting Io to Jupiter. Because of the one-dimensionality, contrary to the 3D MHD, we cannot model the reconnection process per se but the 1D is well suited to study the Alfven wing structure, which provides information on the likely formation of $\boldsymbol{E}_{//}$ and on its magnitude, as we will show latter.

Focusing on the Alfven wave propagation, we simplify the study by neglecting the ionization of Io's cloud neutrals. In this model, friction between the torus plasma and the Io's neutrals provides the only source for Alfven wave but with a reasonably correct magnitude. In the code, the friction is switched on during the time needed for the plasma flow close to Io to travel across its diameter. After this interaction time, the friction term is switched off and the Alfven wave is free to propagate along a field-line detached from Io. This 1D modeling is thus the modeling of the lifetime of a field line: plucked by Io at t=0, interacting with Io through friction during the interaction time and then free again, moving downstream of Io (see Figure 19).

When this particular field line is detached from Io, another field line, upstream, will experience exactly the same interaction with a time delay (dashed field-line on Figure 19), provided that the Io/torus interaction doesn't suddenly change in time. Thus, by stacking parallel field lines side by side at different state of their interaction with Io, we can easily build a 2D mapping of the propagation of the Alfven wave while Io is orbiting in the torus, implicitly assuming that the Io/torus interaction is not changing in time and that the field lines don't interact with each other. This gives a better view of the Alfven wing, comparable to the Figure 15 of the

3D model showing the Alfven Wing propagation. This 2D mapping is the tool we are using in this chapter to study of the Alfven wave propagation.

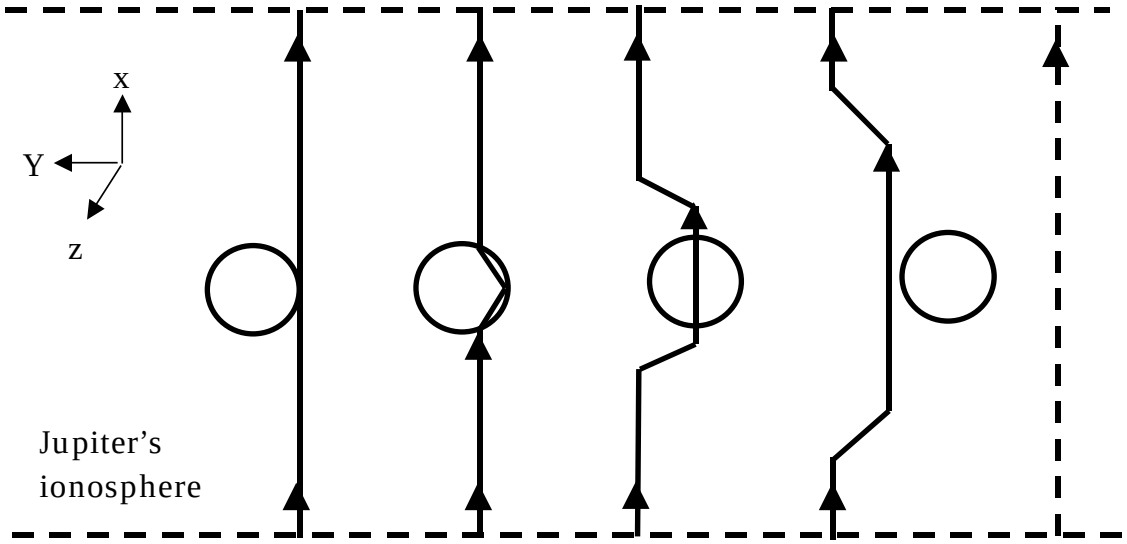

Figure 19: A time sequence of the "life" of a field line as modeled in the1D code.

The 2D mapping provides the following pieces of information:

1. The Alfven wave propagation is correctly addressed in this 2D mapping, providing that each field line interacts with Io the same way as the former one did. This is a limitation of this 2D mapping that means that we don't consider any time variation in the interaction term, like a sudden change of location of Io in the torus, or a sudden change of neutral supply etc.

2. We can get some 3D information even if the 3D dynamics, such as the plasma flow around Io or the magnetic field component out of the XY plane, is not included. We may consider different planes parallel to the XY plane in Figure 19: the plane at Z=0 is the plane where Io interacts with the torus. In this plane, there is a large Alfven magnetic component perpendicular to the Jovian magnetic field (By in the reference system of Figure 19). The planes at $Z = \pm 1\ R_{Io}$ are located on the flanks of Io: in this planes there is no perturbation by Io (no B_y). It doesn't matter for this argument whether those planes are actually located at the edges of Io at 1 R_{Io} or further away. The precise location depends on the size of the neutral cloud that experiences friction. What matters is that the magnitude of B_y actually represents the magnitude of the **sheet current** $\boldsymbol{K}_{//}$

flowing on one side of Io, which is the current density integrated all the way through the Z-direction where some B_y perturbation exists (i.e. from Z=0 to Z= 1 R_{Io}):

$$K_{//} = \int_{z=0}^{z=1RIo} J_x dz = \int_{z=0}^{z=1RIo} \frac{\partial B_y}{\partial z} dz = B_y(z=0)$$

Because of the symmetry, there is also a sheet current on the other side of Io, with the same magnitude but opposite sign (integration from Z=0 to Z= -1 R_{Io}). In this 2D mapping approach, the real width of the current sheet is not addressed; it may even be structured in many extremely thin current sheets. We don't have access to the current density, which is one important parameter for the formation of $\boldsymbol{E}_{//}$ because it triggers the anomalous resistivity just like in the 3D code. Anyway, it will be shown in the next chapter that the sheet current $\boldsymbol{K}_{//}$ (or By magnitude) provides information about the free energy available for reconnection or in other words, for the magnitude of $\boldsymbol{E}_{//}$. The magnitude and location of $\boldsymbol{E}_{//}$ depends on other factors like the convergence of the Jovian magnetic field and the plasma density along the field line, but we will address these issues in the next chapter. **In the 2D mapping of the Alfven wing, as a first approximation, we will interpret the location with the largest magnetic perturbation as the location where there is the largest free energy available for particle acceleration if some anomalous resistivity is triggered.**

In this chapter, we will review the equations of the model, show simple examples of the Alfven wave propagation then run some sensitivity experiments: We will run the code for longer periods of time, change the location of Io in the torus and add some density inhomogeneity to look for possible interferences in the Alfven wave propagation.

5. 2. 1D MHD Model

5.2.1. Geometry of the simulation

The geometry and reference frame are illustrated on Figure 19**. Note that it is not the same as the one used for the 3D simulation**. The field line crossing Io's orbit is a straight line, 480 R_{Io} long, running from the southern Jovian ionosphere at X= - 240R_{Io} to the Northern ionosphere at

X= + 240 R_{Io}. The X-axis is in the direction of the Jovian magnetic field B_0. The Y-axis is in the direction of the corotating plasma and the Z-axis points out of the page.

5.2.2. Description of the magnetosphere

Here we describe the magnetic field and plasma density profile that we consider in the 1D MHD model.

The variation of the plasma density along the field line crossing Io's orbit is illustrated on Figure 20. This profile was computed by Bagenal (personal communication), based on Voyager 1 measurements (see section 2.2 for the description of the torus density and references). Because of the Jovian magnetic tilt, Io moves up and down the centrifugal equator (X=0) by distance of ~ ± 40 R_{Io}.

The variation of the magnetic field along the same field line is computed with the GSFCO4 and magnetodisc model. (Bagenal, personal communication). This model is described in section 2.1, with references. The field magnitude profile is illustrated on Figure 21 and compared with a dipole field. A 1D code doesn't allow for any variation of the magnetic field as $\nabla \cdot \boldsymbol{B} = \boldsymbol{0}$. Thus, we take this varying field effect into account in the density profile itself: we divide the density by the square of the magnetic field so that, keeping a uniform Jovian magnetic field, we get an Alfven velocity varying along the field line consistent with the plasma density and magnetic field variations.

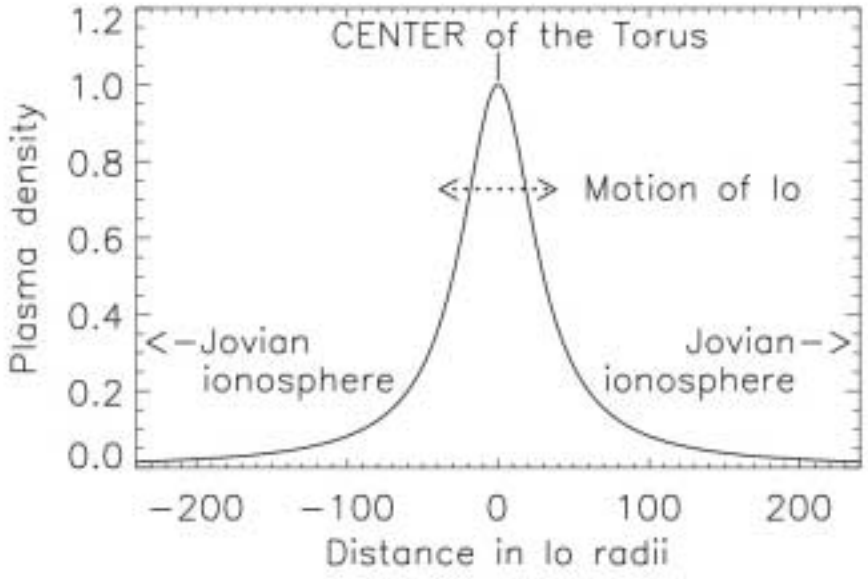

Figure 20: The plasma density profile along the field line crossing Io's orbit. Io is at the center, in the magnetic equator and the Jovian ionospheres are located at X= -240 R_{Io} and +240 R_{Io}. The profile was normalized to 1, its maximum value in the centrifugal equator=52,000 amu/cm^3.

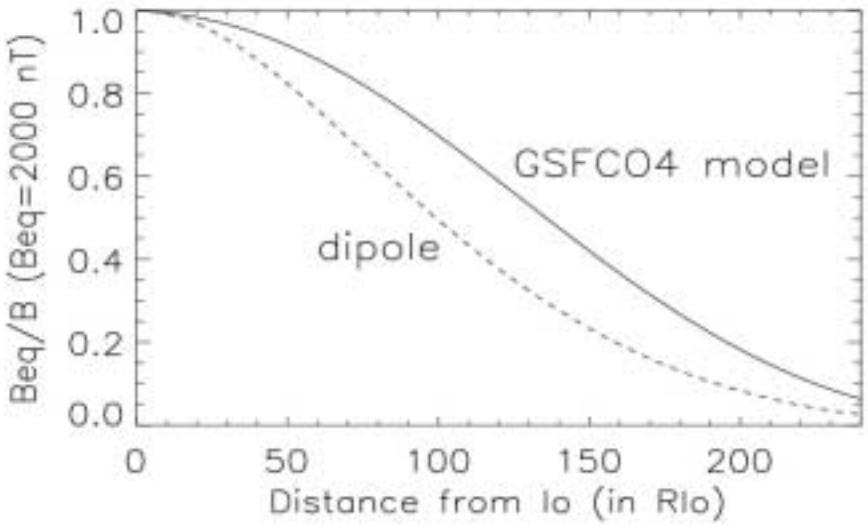

Figure 21: The magnetic field profile along the field line crossing Io's orbit. The plot is normalized to the magnetic field at Io~ 2,000 nT and compared to a dipole field.

5.2.3. MHD equations

The following equations are written in their normalized version (see next section) and solved with a finite-difference leapfrog scheme, which is second order accurate in space and time.

1. The plasma continuity equation doesn't include the ionization of the neutrals

$$\frac{\partial \rho}{\partial t} = -\nabla . \rho \boldsymbol{u}$$

2. The plasma momentum equation includes a friction term Q^P. This friction term depends on:

- The geometrical size of Io θ : the size of the interaction along the field line is about the size of the moon itself.
- The relative velocity between the plasma and the Io.
- A time switch: the friction term is switch on at time=0 and is automatically switch of when the plasma flow has crossed the Io diameter: when $\int \boldsymbol{u_y} dt = 2R_{Io}$
- A collision frequency ν_{coll}

$$\frac{\partial \rho \boldsymbol{u}}{\partial t} = -\nabla . (\rho \boldsymbol{u}\boldsymbol{u}) - \nabla p + \boldsymbol{J} x \boldsymbol{B} + \boldsymbol{Q^P}$$

$\boldsymbol{Q^P} = -\theta \nu_{coll} \rho [\boldsymbol{u} - \boldsymbol{u_{Io}}]$: The friction term as loss of momentum.

3. The energy equation includes the friction terms as well:

$$\frac{1}{(j-1)} [\frac{\partial p}{\partial t} + \nabla . p\boldsymbol{u}] = -p \nabla . \boldsymbol{u} + Q_1^E + Q_2^E$$

$Q_1^E = \theta \nu_{coll} \rho [\boldsymbol{u} - \boldsymbol{u_{Io}}]^2$: gain of energy due to collision of the plasma bulk flow

$Q_2^E = -\theta \nu_{coll} \sigma_{th} [T_{Io} - T]$: loss of energy to heat the neutrals

4. The system is closed with the ideal gas law:

$$p = \rho k T$$

5. Faraday's law and ideal Ohm's law:

$$\frac{\partial \boldsymbol{B}}{\partial t} = -\nabla \mathrm{x} \boldsymbol{E}$$

$$\boldsymbol{E} = -\boldsymbol{u} \mathrm{x} \boldsymbol{B}$$

6. Boundary condition at the Jovian ionosphere: Contrary to the 3D simulations, the 1D code doesn't include a Jovian ionosphere. The ionosphere is taken into account as a boundary condition at X= ± 240 R_{Io} by prescribing the ionospheric integrated Pedersen conductivity $\boldsymbol{\Sigma_P}$. The integrated Pedersen conductivity of the Jovian ionosphere is poorly known. It may vary between 0.2 and 10 mho depending on the ionization sources (Stroebel et al., in Dessler, 1983). For most of the following simulations, we choose a perfectly reflecting ionosphere with

$\boldsymbol{\Sigma_P}$ = infinite. This choice has to be justified. If some reconnection occurs close to Io, particles are accelerated in the vicinity of Io and precipitate in the ionosphere. This precipitation would ionize further the ionosphere and increase the ionospheric conductivity under the Io spot. Later on, when the Alfven wave reaches the upper part of the Jovian atmosphere, the ionosphere has been prepared by the Io spot and thus presents a higher conductivity, making it close to perfectly reflecting. However, in this 1D approach, which doesn't include an ionospheric density profile, the choice of the resistivity value is not critical: Chosen between 1 and 10 mho, it is always much larger than the Alfven conductivity at the top of the Jovian ionosphere:

$$\Sigma_A = 1 / (\mu_0 * V_A) \sim 0.05 \text{ mho}$$

It will be shown in section 5.3.2 that the Jovian ionosphere absorbs the wave if the integrated Pedersen conductivity is close to the Alfven conductivity at the ionosphere. Thus a perfectly reflecting ionosphere is in a general way justified by the observed Io spot brightness and, in this particular 1D code is anyhow a good approximation.

5.2.4. Numerical parameters and normalization

All quantities have been made dimensionless by normalization to typical values close to Io, similar to those presented in section 4.3. In particular, we use the same collision frequency as in the 3D code (see section 4.3 "Numerical parameters and normalization"), based on the total ionization rate measured by Galileo (Bagenal, 1997). This collision frequency is small which

means that the field lines are not frozen to the Io neutral cloud: The torus plasma flow is slightly slowed down by the friction with the Io's neutrals and the field lines cross Io's diameter in a time that is slightly longer than the time for the corotation flow to convect past Io. Another consequence of this small collision frequency is that the magnetic perturbation caused by the Io/torus interaction is small compared to the Jovian magnetic field, which fits well with the linear Alfven wave description.

5. 3. 1D propagation of the Alfven Wave, results

5.3.1. Simple example

Here we show an example of the propagation of an Alfven wave through a discontinuity. It is not directly related to the Io/torus interaction: In this simulation, there is no friction term in the fluid equations and we use a uniform background magnetic field. Nevertheless, it will help to better understand the Alfven propagation when the Io/torus interaction will be included, as the torus density profile may be viewed as a continuous succession of small discontinuities. Figure 22 shows the conditions of the simulation before the interaction of the wave and the density discontinuity. We assume a background plasma density with a discontinuity along the background magnetic field: The density is constant = 1 from X= -60 and decreases abruptly to 0.1 at X= -10. The initial velocity perturbation V_y and a magnetic field perturbation B_y are consistent with an Alfven wave propagating from left to right. An Alfven train (which means the V_y and B_y perturbations) is launched to propagate from left to right, toward the density discontinuity. Figure 23 shows the variables after interaction with the discontinuity (t=30 T_0). It shows that part of the train is transmitted with an amplitude decreased by ~ ½ and part of it is reflected toward X= -20. This illustrates that for a decreasing plasma density, the transmitted B_y has the same sign that the incoming Alfven wave, while the reflected B_y changes sign. Consistent with the direction of the Alfven wave propagation, the velocity perturbation V_y, both the reflected and transmitted wave, doesn't change sign. This is important to note for the interpretation of the Alfven wave propagation in the Jovian density torus.

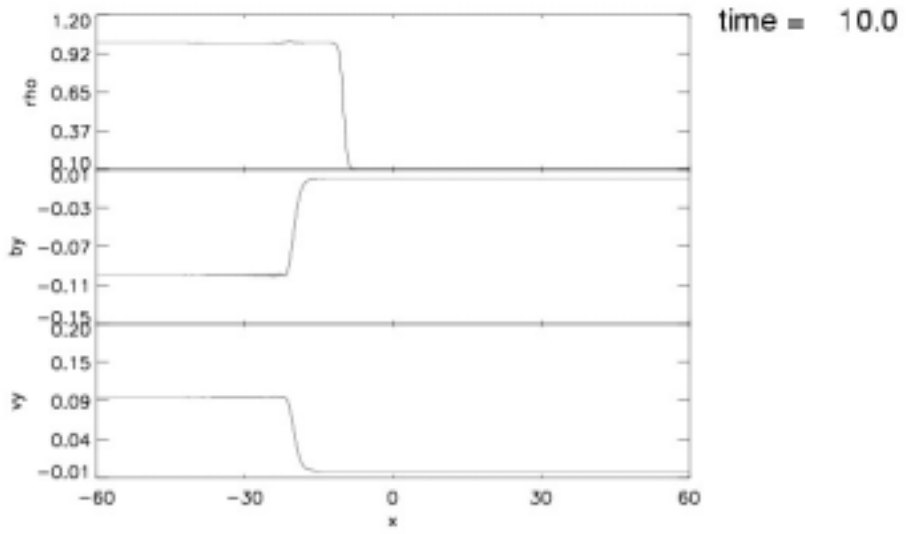

Figure 22: Initial condition of the Alfven train propagation through a discontinuity.

The density discontinuity is shown on the top panel, starting at 1 and decreasing abruptly to 0.1. The magnetic and velocity initial perturbations are shown on the second and third panel. They are chosen to have wave propagation from left to right.

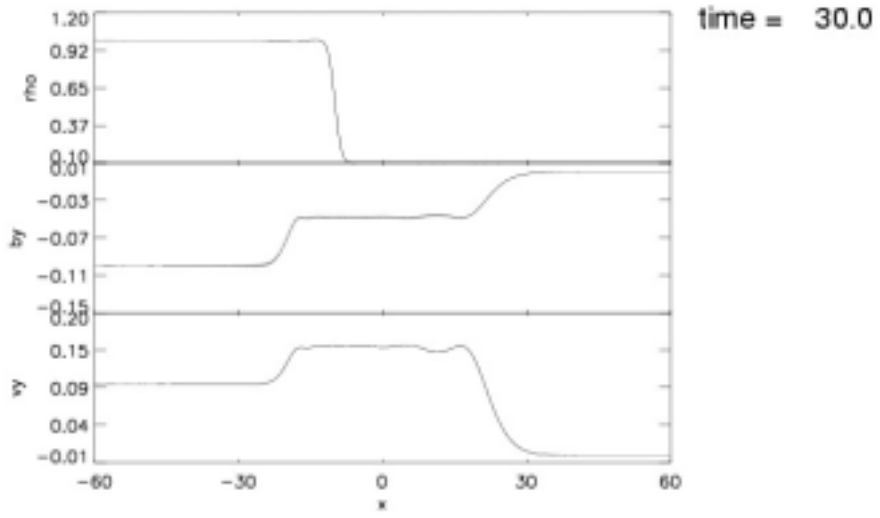

Figure 23: Reflection of the Alfven train on a discontinuity.

The reflected Alfven wave propagates toward the left and, at the time of this snapshot, the front of the wave hits x= -30. The transmitted wave propagates toward the right and the front of the wave reaches x= +30.

5.3.2. Propagation of the Alfven wave in torus/GSFCO4 density profile

Here, we include the friction term and a realistic magnetosphere description.

1. Propagation of Alfven pulse

Figure 24 illustrates the propagation of the magnetic and velocity perturbations B_y and V_y created by the switch-on of the friction term. The first panel shows the background density profile including the varying magnetic field effect and Io (the location of the friction) is in the magnetic equator at X=0. The second and third panels show the magnetic perturbation B_y and the velocity perturbation V_y propagating like pulses toward the southern Jovian ionosphere (X= -240). The symmetric perturbation propagates toward the Northern Jovian ionosphere (X= + 240), consistently with the Alfven propagation: B_y is negative and V_y is positive. The small perturbations behind the Alfven waves are indications of some internal reflection of the wave on its way through the torus. We will address this issue in the next section.

We use this example to compare the computed variables magnitude to the one observed by the spacecraft that flew close to Io.

- The computed interaction is the time needed for the flow around Io to cross Io's diameter. We compute this interaction time to be close to 9 T_0 (~90 sec). It is a little bit more than the time needed for the corotating plasma to flow across Io's diameter (~ 60 sec) because the friction has slowed the flow down.

- The time for the Alfven perturbation to go from Io to Jupiter and back to the middle of the torus is about 130 T_0 (~1,300 sec). This is close to the 1,000 sec round-trip propagation time described in section 3.2 (Open-loop model).

- The magnetic perturbation close to Io is about 0.027 $B_{0,}$ (~54 nT). The Voyager1 measurement of the magnetic perturbation close to the Io flux tube was about 100 nT (see section 2.2).

In general, the computed quantities relative to the Alfven wave propagation are reasonably close to the one observed close to Io.

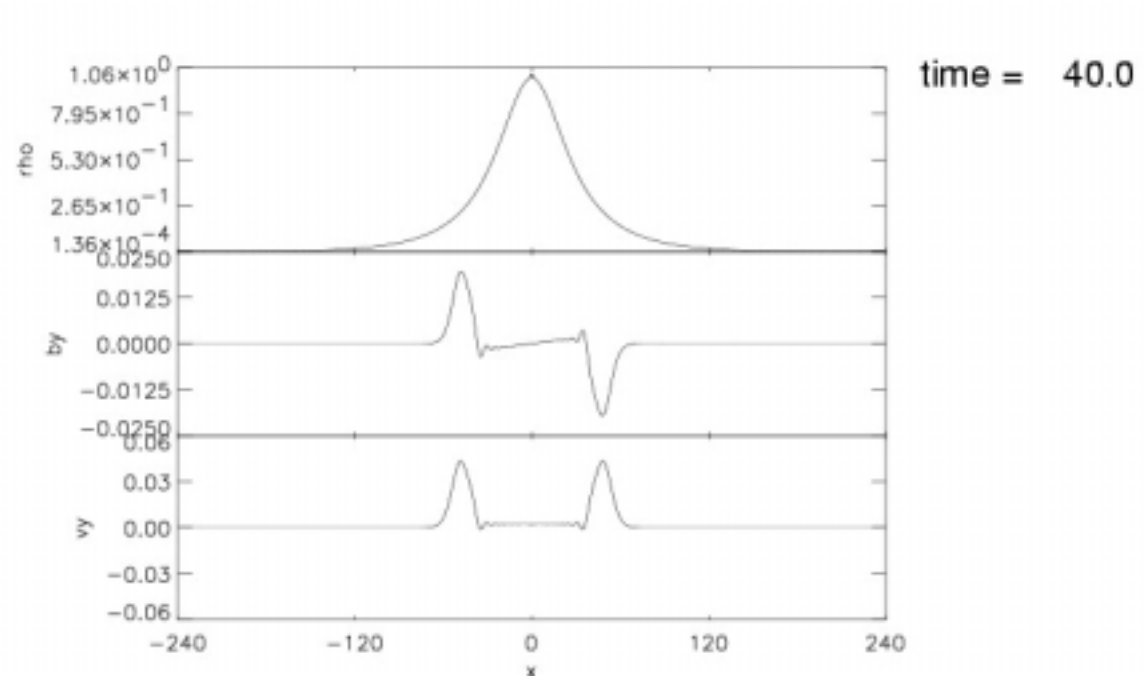

Figure 24: Propagation of the Alfven pulse through the torus.

The pulse close to X= -60 moves toward the left and the pulse at X= +60 moves to the right.

2. Internal reflection

Section 5.3.1 illustrated the reflection of an Alfven wave in a density discontinuity. The rational for this illustration is based on the idea that a density gradient is somewhat comparable to a continuous succession of small discontinuities. We might thus expect that when the wave travels through the torus density profile, it experiences some reflection. This idea is not new and has been addressed by several authors. Wright (1987) showed that most of the Alfven wave energy is reflected on its way through the torus by the plasma density gradient. He computed that only 25% of the Alfven wave energy would reach the Jupiter's ionosphere. In a recent article, Crary (1997) claimed that the Alfven wave doesn't reach the ionosphere at all. This statement is important in the context of the acceleration process that we propose in this thesis. If the wave doesn't reach Jupiter's ionosphere, then the acceleration of particles cannot be close to the

ionosphere as it happens in aurora on Earth but must occur in the magnetosphere. It is worth examining this result more closely. We thus compute the amount of energy reaching the ionosphere with this 1D MHD code, following Wright (1987) method: We compute the time integrated *Poynting flux P(x,t)* of the Alfven wave:

$$P(x,t) = \int_0^t u_y(x,\tau) B_y(x,\tau) B_0 \, d\tau$$

A wave propagating toward X = -240 has a positive integrand while a reflected wave has a negative contribution to this time-integrated Poynting flux. As far as an Alfven pulse is propagating without any reflection, then *P(x,t)* is constant as soon as the wave reaches the location x. When a part of the Alfven pulse is reflected on its way down to the torus, it will be detected by a decrease of *P(x,t)* due to the negative contribution of the reflected wave. In order to focus on the internal reflection only and to avoid the perturbation of the wave reflected on the Jovian ionosphere, we follow Wright (1987) in using a perfectly absorbing ionosphere. This condition is satisfied if the integrated Pedersen conductivity of the Ionosphere is equal to the Alfven conductivity at the ionosphere. It can be shown that the reflection coefficient of the Alfven wave on the ionosphere is

$$C_r = \frac{B_y^r}{B_y^i} = \frac{\left(\Sigma_p - \Sigma_A\right)}{\left(\Sigma_p + \Sigma_A\right)}$$

with

$$\Sigma_p = \Sigma_A = \frac{1}{\left(\mu_0 u_A (x = \pm 240\right)}$$

Then C_r=0 if $\Sigma_p = \Sigma_A$ and the wave is completely absorbed in the Jovian ionosphere.

Figure 25 shows a superposition of the profiles of the time-integrated Poynting flux at successive times (labeled from t=0 to t=100). Only one half of the field line is represented here: The Jovian ionosphere is on the left at X=- 240 R_{Io} and Io is in the middle of the torus at X=0, on the right of the horizontal axis. The superposition of the profiles shows a wave propagating from Io toward the Jovian ionosphere. The top view shows the propagation of the Alfven wave in a smooth density gradient. For the sake of illustration, we use here the torus density profile without including the dipole field effect so that the gradient is not too steep. The wave propagates toward Jupiter and is entirely absorbed at the ionosphere: there is no reflection on its way through the

torus. The bottom view shows the same wave, propagating in the torus density including the dipole effect: the resulting density gradient is steeper. This plot shows that, with this larger density gradient, the wave is partially reflected on its way through the torus:

- Until time=60 T_0, *P(x,t)* is roughly constant, the density gradient is still relatively smooth and the pulse has traveled down from X=0 to X~ 150 $R_{Io.}$

- At time=70 T_0, the pulse has reached the ionosphere, but the density gradient is sharp relative to the size of the pulse and some of it is reflected by the density gradient.

- At time = 80 T_0, some part of the pulse has been reflected back by the torus density gradient and travels toward the torus center at X ~50 R_{Io}. *P(x,t)* is constant at the ionosphere (X= -240 R_{Io}), showing that there is no energy moving down in the ionosphere any more. After that time, *P*(X= -240 R_{Io}) is about 40 % of *P*(X=0) at time=0. Only 40 % of the energy of the wave has reached the Jovian ionosphere during its first travel down the field line, the rest has been reflected by the density gradient.

- The percentage of the energy reaching the ionosphere depends on the density profile used and of the size of the pulse (Wright, 1987; Wright, 1989) but we confirm Wright's results: a substantial part of the Alfven wave is transmitted through the torus and reaches the ionosphere. If the Alfven wave reaches the ionosphere, then we cannot rule out that some reconnection happen close to the planet depending on the magnitude of the magnetic perturbation, as will be shown in the next chapter.

- From this simulation and the 5.3.1 simulation of the propagation of an Alfven wave in a discontinuity, we expect that when the Alfven wave propagates in the torus density profile, there is substantial reflection on the density gradient and a change of the sign of the magnetic component of the reflected wave compared to the incoming wave.

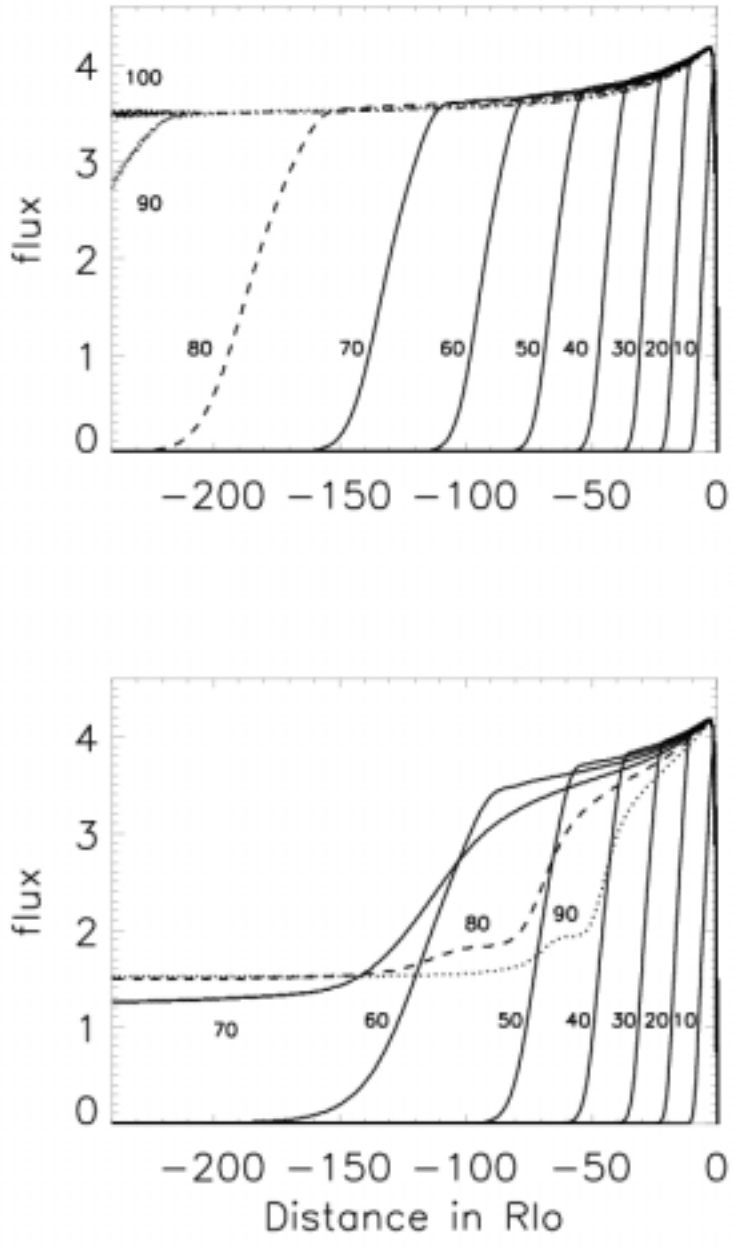

Figure 25: Snapshots at the time integrated Poynting flux.

The ionosphere of Jupiter is on the left (X=- 240) and Io is on the right. Top view: propagation of the wave in a smooth density gradient. Bottom view: propagation of the wave in a density gradient including the dipole effect: some part of the wave is reflected on the density gradient. The flux units are multiplied by 10^3.

5. 4. 2D mapping

As explained in the introduction, we map the propagation of the Alfven wave in the X-Y plane by stacking, side-by-side, several parallel field lines at different states of interaction with Io. The resolution of this mapping is $0.5R_{Io}$ in both directions. Let's recall that we can interpret the magnetic perturbation as the total sheet current flowing on one side of Io. Because of the symmetry, the same sheet current is flowing on the other side of Io with a reversed sign. But, as a first approach, the location of the largest magnetic perturbation is also interpreted as the location of the largest free energy available for accelerating particles on both sides of Io.

5.4.1. First example: The " flat" torus

To compare with the 3D simulations of section 4.3, we run a simulation with a uniform background plasma density and a uniform Jovian magnetic field. Figure 26 shows the mapping of the magnetic perturbation B_y after a time= 96 T_0. The Jovian field lines are vertical, extending from the southern ionosphere at X= -240, crossing the Io's orbit in the centrifugal equator at X=0 and reaching the Northern Jovian ionosphere at X= + $240R_{Io}$. The horizontal axis represents the distance traveled by Io on its orbit. During the time of the simulation, Io traveled a distance ~ 24 R_{Io}. This distance is actually expressed in degrees of sub-longitude. This conversion is estimated from a projection of the Io's radius on Jupiter's ionosphere, using the VIP4 model, when the observed Io spot is close to 70^o latitude (Clarke, personal communication). This computation may seem awkward but as the magnetic field is not a dipole, this is a reasonable way to compute a *lead-angle* or an *observed shift angle* that can be directly compared to those observed in the IR or UV pictures of the Io spot. We estimate that a distance of ~ $6R_{Io}$ along Io's orbit corresponds to a sub-longitude distance of 1^o while the same estimation for a simple dipole field would lead to $4R_{Io}$ per degree, resulting in too large an *observed shift angle.*

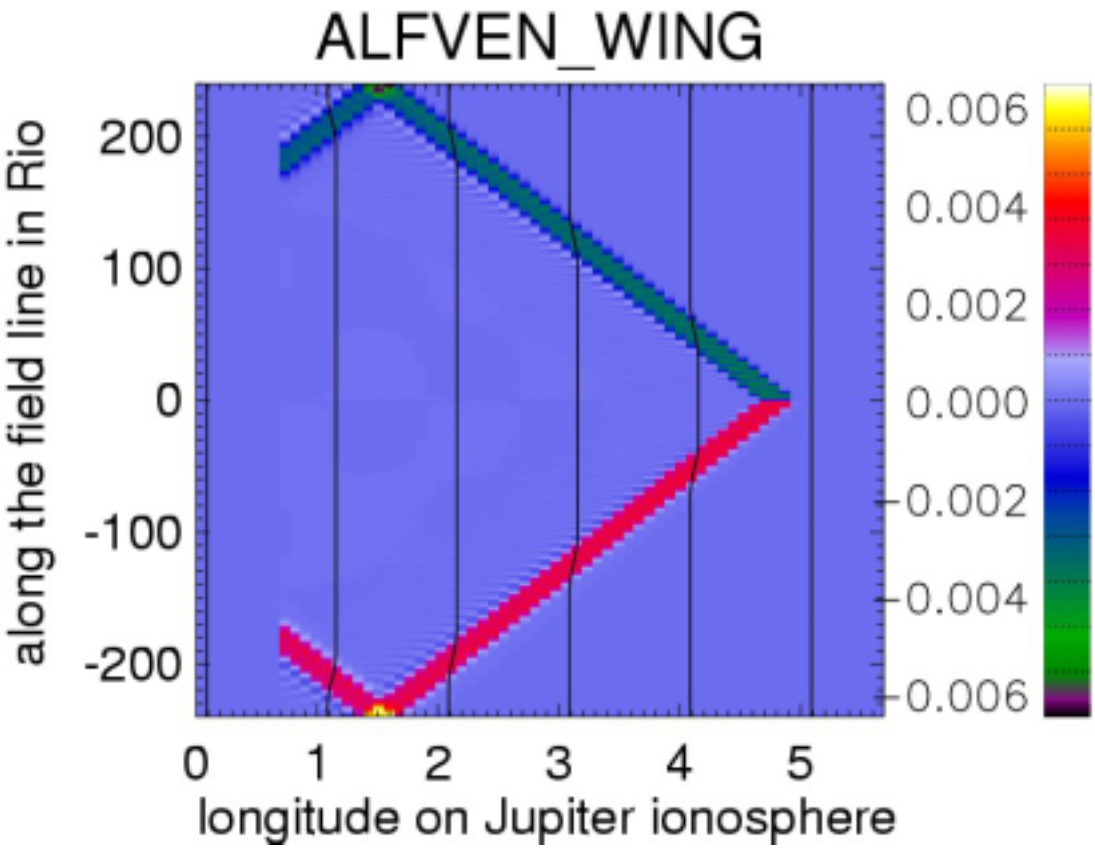

Figure 26: Propagation of the Alfven wing in the "flat torus".

This graph shows the magnitude of B_y.

- This magnitude, as well as the M*ach-angle*, is constant all along the Alfven wing from Io to one of the ionospheres and is similar to the 3D MHD results shown on Figure 15. The field lines are superimposed as vertical black lines that show a small bending in the wing caused by the Alfven wave perturbation.

- B_y is maximum close to the ionosphere of Jupiter because we assume here a perfectly reflecting ionosphere of Jupiter ($\Sigma_p = \infty$). The reflected B_y has the same amplitude as the incoming B_y and the resulting magnetic perturbation at the ionosphere is twice the incoming one. If we were to use a smaller integrated Pedersen conductivity, this local maximum would not exist.

5.4.2. The complete magnetosphere description

We now map the propagation of the Alfven wave, using the magnetic field/torus density profile and compare it to the previous "flat torus" mapping. We will assume that the ionosphere is perfectly reflecting.

1. Alfven wing with Io in the center of the torus

Figure 27 shows the same display as the previous one with a different color scale after a simulation time t= $96T_0$.

- The Alfven wing is now curved and the magnitude of the B_y perturbation is no more constant along the wing. This is a consequence of the increasing Alfven velocity along the field line: Further down the wing, the *Mach-angle* decreases and is almost $=0^o$ close to the ionosphere. The magnitude of the Alfven perturbation B_y decreases as well.

- The maximum of the B_y perturbation occurs close to Io where the plasma density is large.

- The Alfven wave is reflected on the perfectly reflecting ionosphere, keeping the same sign: the reflected wing is red in the northern hemisphere and blue in the southern hemisphere, just like the incoming wing. There is no apparent local maximum close to the ionosphere any more.

- There is substantial reflection of the Alfven wave on the torus density gradient. Remember that in the simple example of section 5.4.1, we showed that an Alfven wave propagating through a discontinuity where the density decreases is reflected with a change of sign. The same kind of reflection is illustrated by the red pattern that precedes the reflected blue wing in the north hemisphere (X>0) and by the dark blue pattern preceding the reflected red wing in the southern hemisphere (X<0).

- The ***lead-angle*** of this Alfven wing depends now of the whole density profile and is close to 3^o but as the maximum of B_y occurs very close to Io, in the context of our first order interpretation, the *observed shift angle* would be ~ 0^o.

- The magnitude of the magnetic perturbation represents also the sheet current flowing on one side of Io. Because of symmetry, the same current flows on the other side of Io with a reversed sign, showing the same pattern as the one displayed in this figure, but with reversed colors.

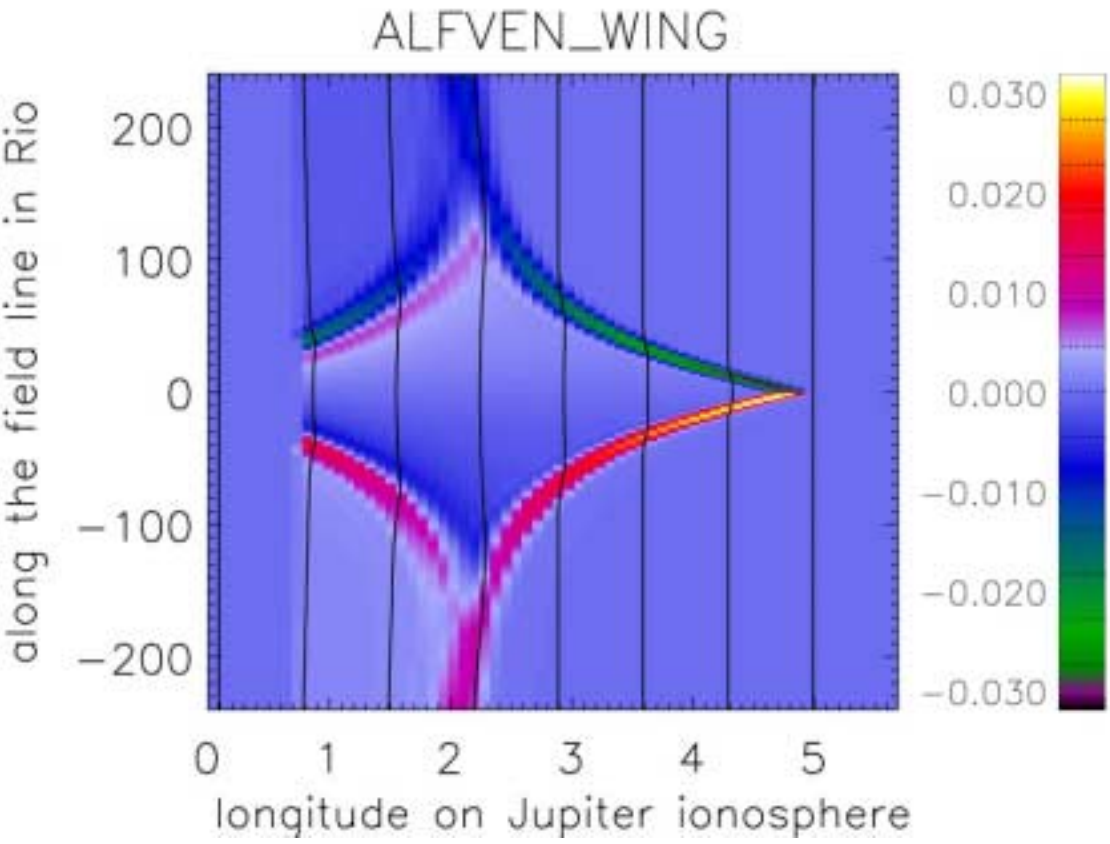

Figure 27: Propagation of an Alfven wing in a full magnetosphere description.

- The magnitude of the magnetic perturbation is quite small because the collision frequency deduced from Galileo measurements is small (see comments in section 5.2.4). In Figure 28, we illustrate the magnetic perturbation for a collision frequency 10 times larger and compare the results to Figure 27. Figure 28 shows the Alfven wing after $60T_o$, smaller than in the former figure. Because of the increased collision frequency, the torus plasma flow is more slowed down by the Io's neutral, the magnetic field is stuck close to Io during a longer time, it is more frozen to Io and the field line perturbation is larger: the field line follow the Alfven wing for some distance.

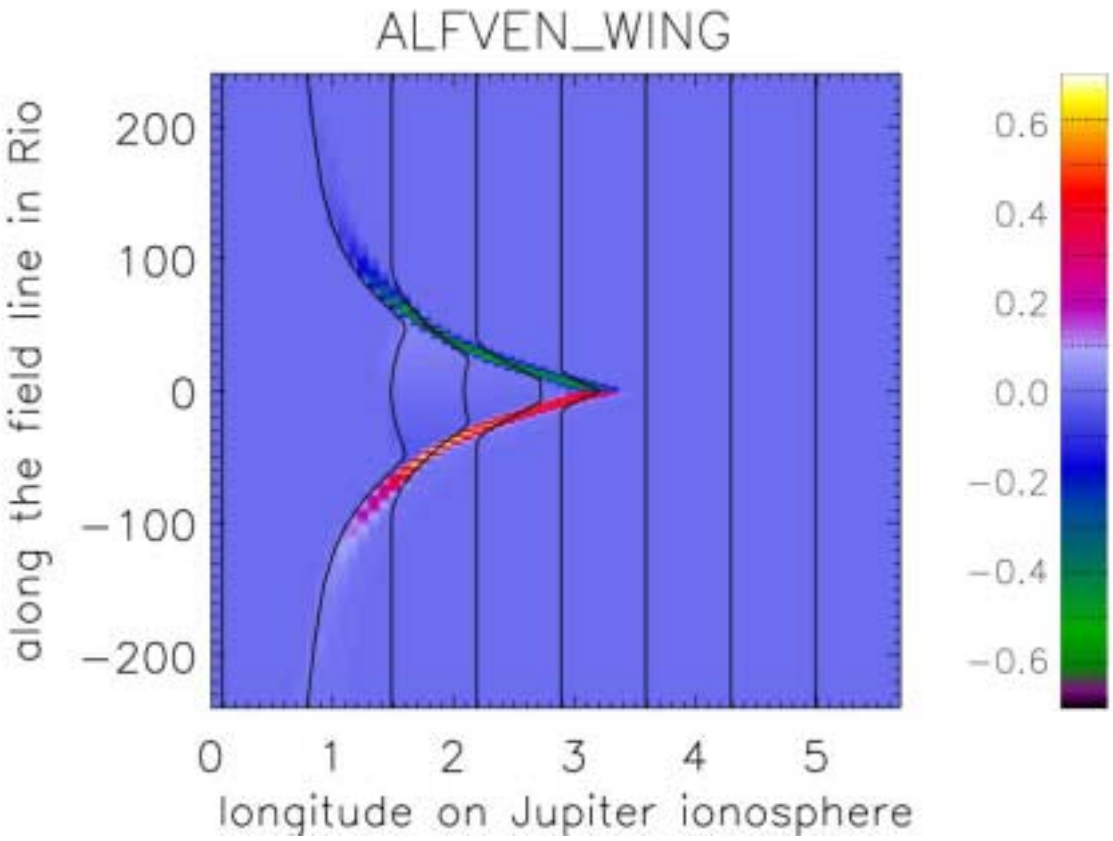

Figure 28: Alfven wing for an increased collision frequency.
This mapping shows the Alfven wing at an earlier time (60 T_0) than the former figure.

2. Longer run with Io in the center of the torus

Figure 29 shows the same simulation but after a much longer time (time = 148 T_0). The reflected Alfven wings travel back to the middle of the torus were they interfere, creating multiple maxima of the magnetic perturbation, separated by ~ 6°. This is, formally, reminiscent of the multiple Io spots observed in 1998 and 1999 in the IR and UV, which were separated by 3° to 5°. But this conclusion is based only on the free energy available for the acceleration (The magnitude of the magnetic perturbation). It should be recall that the location of the Io spots and thus, of the formation of a parallel electric field doesn't depend only on the free energy available, as will be shown in the next chapter. Let's take this example as a hint that **any structure in the observed Io spot is likely related to a structure in the Alfven wave propagation**, like the multiple maxima of the free energy caused by multiple reflections as illustrated here.

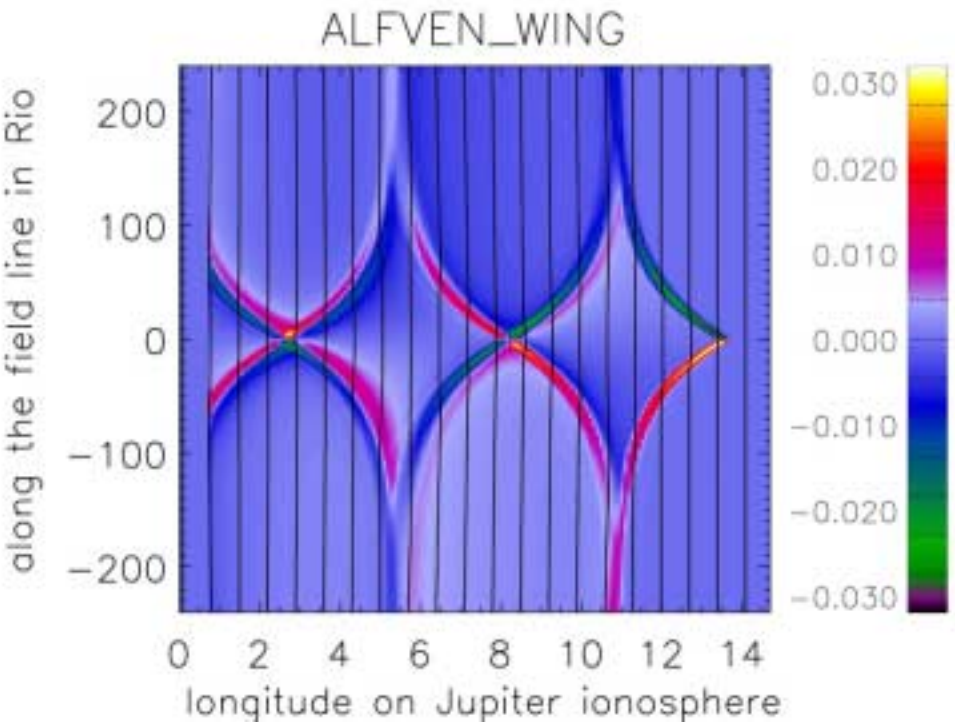

Figure 29: Interference pattern of the reflected Alfven wings. Multiple maxima occur in the center of the torus.

3. Io in the northern part of the torus

Figure 30 shows the same long-run simulation when Io, on the course of the torus rotation, is in the northern part of the torus.

- The By maxima appear always in the center of the torus, where the plasma density is large. Because of the asymmetric location of Io relative to the high-density core of the torus, the south *lead-angle* is larger ~ 3.5^o and the north *lead-angle* is smaller ~ 1.5^o than in Figure 29.

- The maximum amplitude of B_y is smaller than when Io is in the center of the torus as shown by the color scale. Io encounters less dense plasma and the friction is smaller. If the parallel electric field is formed where the sheet current $K_{//}$ (or By) is large, then the *observed shift angle* and brightness of the Io spot in the southern and northern hemispheres should be anti-correlated. In our simulation, when Io is in the northern part of the torus, the south *observed shift angle* is about 1.5^o and is close to 0^o in the north. This is reminiscent to the Clarke et al. (1996) observation where they found an anti-correlation between the *observed shift angle* in the north

and south hemispheres. They couldn't find any trends for the Io spot brightness variation (see section 3.3.3).

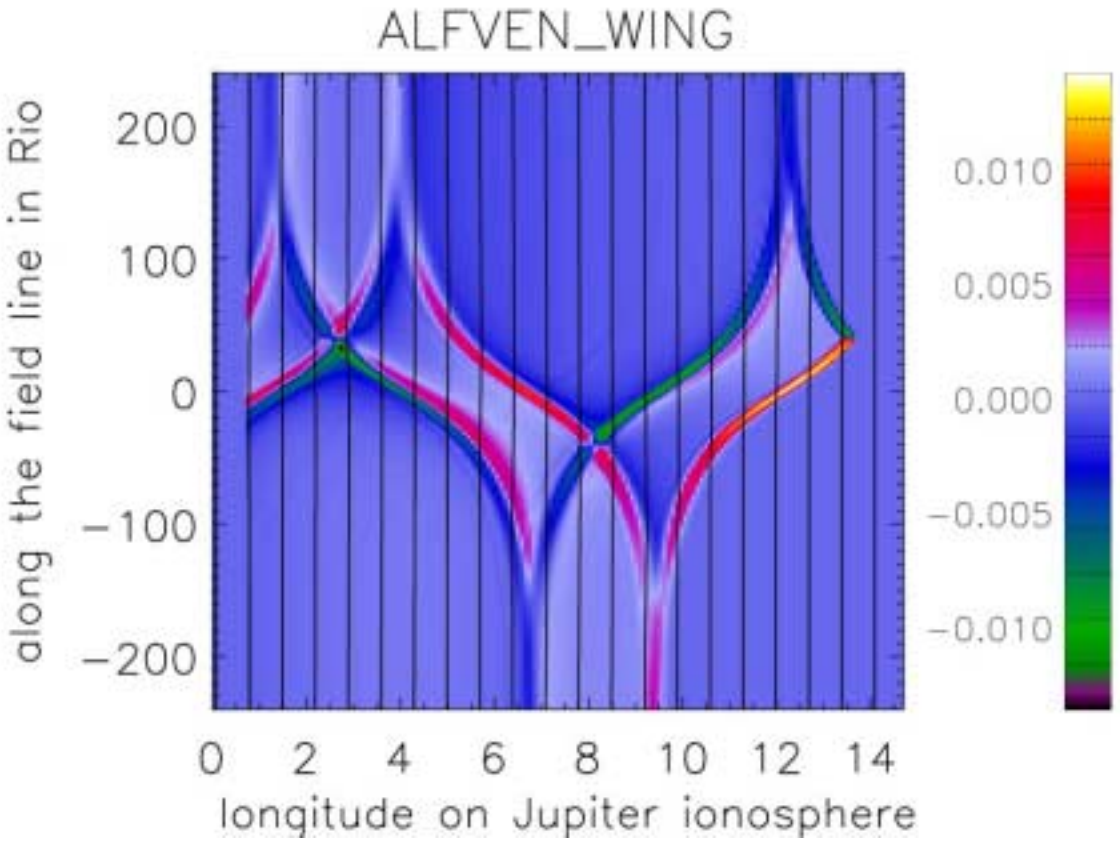

Figure 30: Interference pattern when Io is on the side of the torus. Io is located at X= +40 Rio, in the northern part of the torus.

5.4.3. Inhomogeneity in the torus density

A density inhomogeneity in the plasma torus will further complicate the interference pattern. We simulate this situation, assuming a local increase of the torus plasma density at X=+ 120 R_{Io}. The local density is 3/2 of the density in the torus center, and has a gaussian shape with a full width at half maximum of 20 R_{Io}. Some inhomogeneity in the torus was observed by Voyager 1. In section 2.2, dedicated to the description of the torus, we pointed out that, during the Voyager 1 flyby, a thin high-density structure called the ribbon was detected close to Io's orbit.

The ribbon moves between 5.6 and 5.9 R_J, has a large local density (~3000 pcl/cm^3 to be compared to the torus center density ~2000 pcl/cm^3), is thin ~20 R_{Io}. During the ~13-hour torus rotation period (in Io's frame of reference), Io moves up and down relative to the centrifugal equator. It is thus plausible that Io might be above/under this density blob, depending on Io's phase angle. The maximum distance between Io and the ribbon should be < 30 R_{Io}. To make the point clearer, we locate the blob further down the torus at a distance of 120 R_{Io} from the moon.

Figure 31 shows the pattern of interference resulting from reflections through the torus density profile and through the high-density blob. The purpose of this simulation is merely to show that any density inhomogeneity in the torus produces multiple location of B_y maxima. If the acceleration location is close to these B_y maxima, we might expect to observe a train a multiple-spots auroral emission in the Jovian ionosphere, irregularly spaced because of the multiple irregular angles that the interferences produce. Once again here, our goal is to show that any structure in the Alfven wing propagation (here irregular interferences) is likely to cause a structure in the Io's related auroral emissions.

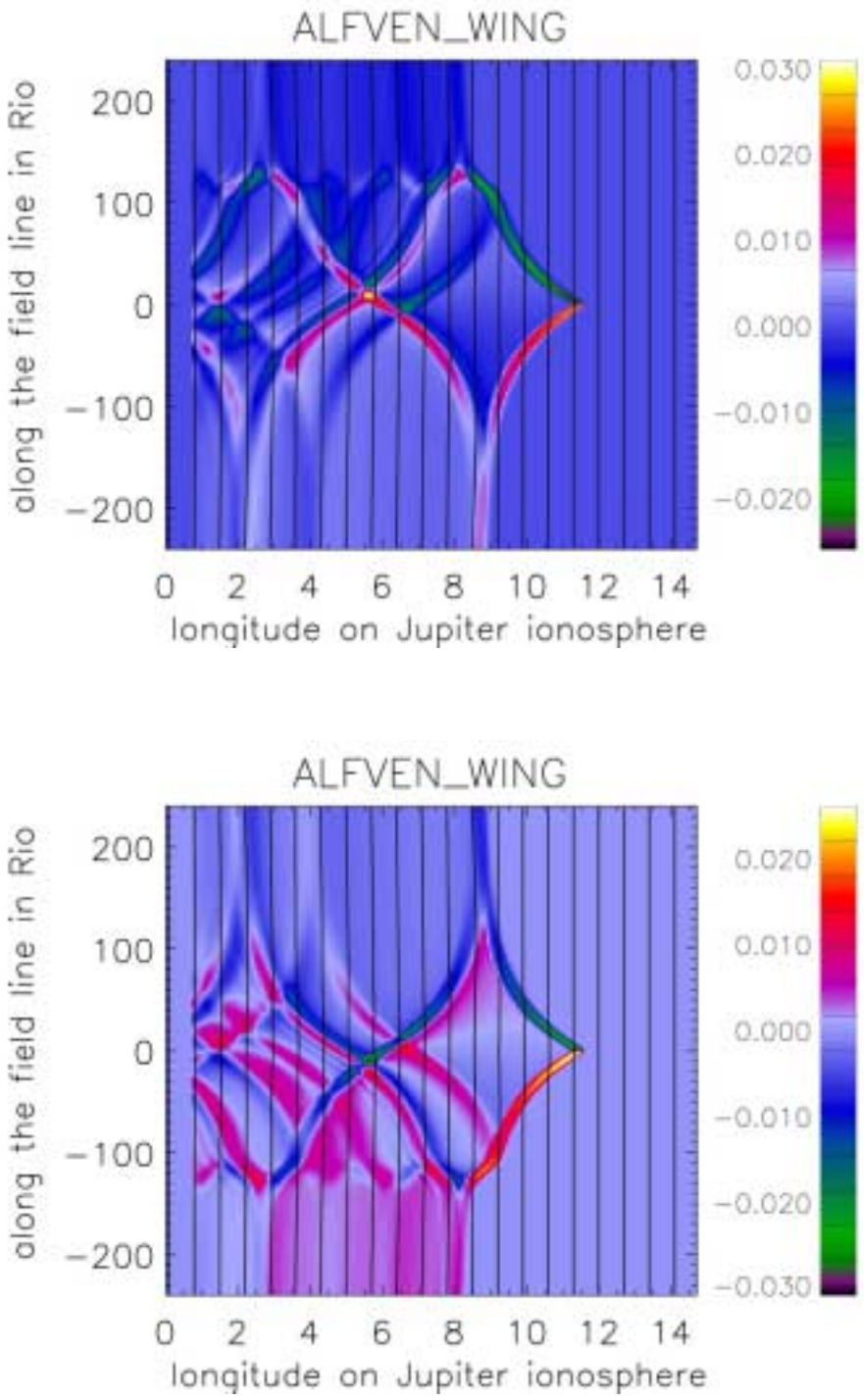

Figure 31: Interference pattern caused by a density inhomogeneity in the torus.

Top view: The density blob is located at X=+120. Bottom view, the blob is at X= - 120. Note that the color scale is different for each plot.

5. 5. Conclusions

In this chapter, we focused on the Alfven wing propagation in a more realistic description of the magnetosphere. We made some sensitivity experiments like changing Io's location in the torus and adding a density blob in the torus. We had in mind the simple picture that the magnitude of the magnetic perturbation or the free energy might be important for acceleration processes. In this first approximation, these results show an acceleration process that takes place in the center of the torus where the plasma density is the largest. In this case, the Io-spot should likely show a multiple-spot structure with an angular separation ~ 6^o (It should be noted that these simulations don't take into account the fact that the formation of a parallel electric field somewhere along the Alfven wing will reduce the magnetic perturbation and that there will be less free energy available for further formation of multiple acceleration electric field). The *observed shift angle* of the first spot should be very small (close to 0), should vary with the location of Io relative to the magnetic equator and present a north/south anti-correlation.

The main result of this chapter is that any structure in the Alfven wing propagation (like interference due to multiple reflections at the ionosphere or existence of a density inhomogeneity or asymmetry of the location of Io in the torus**) is likely to cause a structure in the Io related auroral emission**. **The Io auroral observations support this idea**. In the observations described in section 3.3, the Io spot emission is indeed sometimes structured as multiple spots, separated by 3 to 5^o, specifically when Io is close to the center of the torus. The *observed shift angle* of the first spot varies between 0^o and 15^o and shows a north/south anti-correlation consistent with the location of Io in the torus. This seems promising, but the Io spot emission is **not always** structured in multiple spots. Most of the time, only one Io spot is detected followed by a smooth fainting trailing tail. Moreover, if the magnetic models can be trusted, the *observed shift angle* is sometimes as large as 15^o, which is a feature that we can't simulate. Thus the acceleration mechanism, although probably related to the location of large B_y, is clearly more complex.

The picture of the acceleration taking place where B_Y is large is too simple. For instance, we didn't address the issue of the current density, which is the one that triggers the resistivity. The magnitude of the parallel electric field depends on the free energy available but also on the

plasma density. In the next chapter, starting from the simulations we presented here, we study the reconnection process itself in more details.

CHAPTER 6: RECONNECTION STUDY

6. 1. Introduction

In the former chapter, we focused on the Alfven wave propagation. But we are mainly interested in the acceleration process, which means the magnitude of $\boldsymbol{E}_{//}$ and the size of the $\boldsymbol{E}_{//}$ region. In the last chapter, we focused on the free energy available for reconnection and acceleration of particles. The parallel electric field magnitude depends not only on the free energy but also on the plasma density, which has not been taken into account yet. In our model, another important parameter for the formation of the parallel electric field is the current density, as it is the parameter that triggers the anomalous resistivity. So far, we have just computed the sheet current. This sheet current represents the integration of the current density across the Alfven wing. Its magnitude is equal to the magnitude of the Alfven wave magnetic perturbation. In this chapter, we show that the converging magnetic field has an effect on the variation of the current density and thus on the triggering of the parallel electric field formation.

The reconnection process cannot be modeled in a 1D approximation and we cannot obtain the parallel electric field and the reconnection rate directly. We will show that, assuming that the reconnection is in steady state, we can use **scaling laws** for reconnection to obtain **an estimate for the magnitude of the parallel electric field along the field line and for the "efficiency" of this electric field.**

We will start the chapter with the converging-field effect correction of the field-aligned current using the results of the 2D mapping presented in the previous chapter. Later on, we will define the reconnection rate, show that it can be interpreted as the efficiency of the acceleration process and, with the same 2D mapping, we will compute the variation of the reconnection rate.

6. 2. Field convergence effect on the anomalous resistivity

When a current flows along the field line from Io to the Jovian ionosphere, it flows through a flux tube section that decreases as $1/B_0$. Assuming a constant sheet current along the field line, this geometrical effect increases the current density from Io to the Jovian ionosphere. This geometrical effect is sketched in Figure 32. We can look at this effect by simply multiplying the 2D mapping of the B_y perturbation (representing the sheet current) by the variation $B_0(x)$. Figure 33 shows the effect of this geometrical correction: The maximum of the current density is not anymore close to Io. **The conclusion is that the most probable location of switch-on of the anomalous resistivity is close to the Jovian ionosphere**.

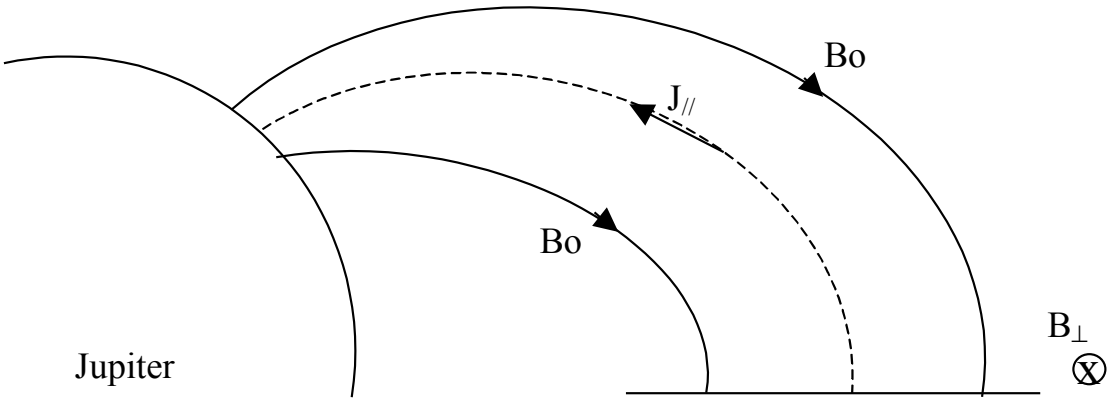

Figure 32: Sketch of the converging-field effect on the current.

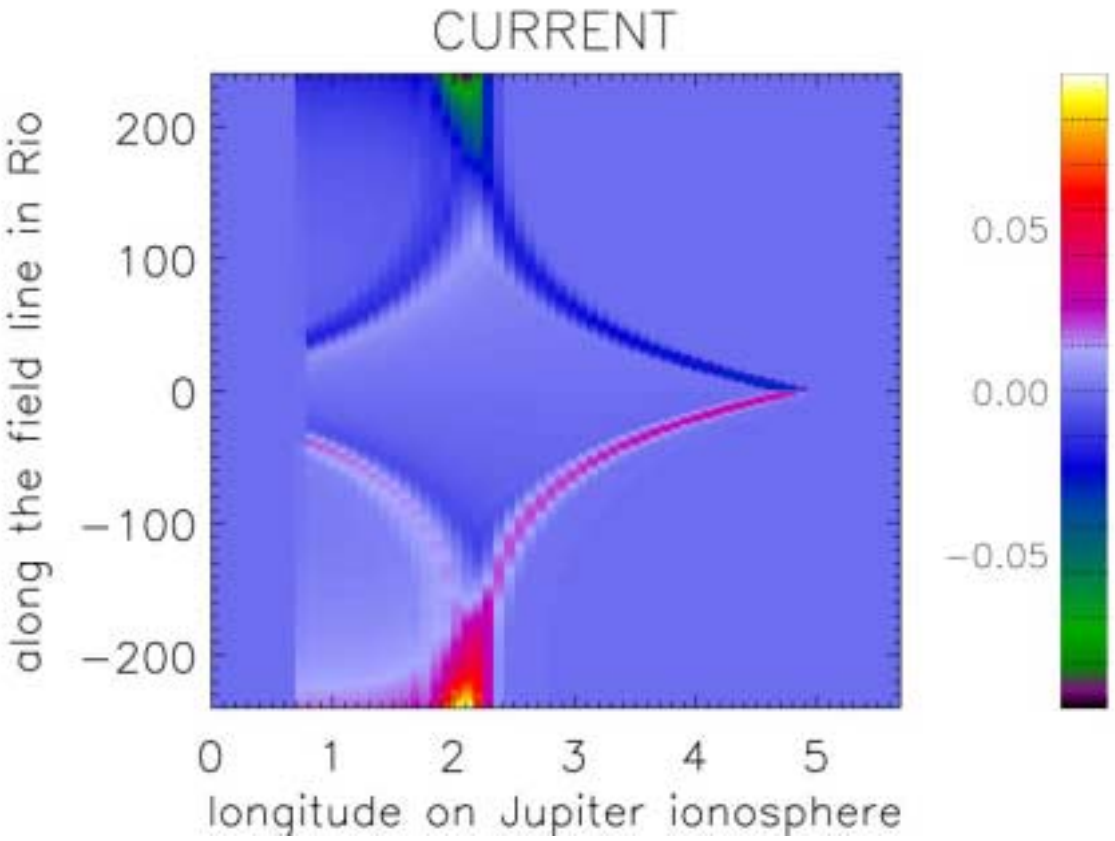

Figure 33: Converging-field effects on the field-aligned current.

6. 3. Micro-instabilities

Throughout this work, we assumed that some anomalous resistivity could be triggered along the field line depending on the field-aligned current density. We haven't addressed the origin of this anomalous resistivity. We merely make the assumption that the field-aligned current might excite some micro-instabilities along the field line and lead to this anomalous resistivity. In this section, our goal is to illustrate this assumption by considering only two micro-instabilities among the zoo of the instabilities that could take place in the Jovian magnetosphere. We use the sheet current computed in the former chapter, the plasma conditions at Jupiter and some assumptions about the current sheet thickness to check if the ion acoustic and ion cyclotron

instabilities could be excited. It will be shown that, considering the physics and the spatial resolution of our model, these instabilities cannot be excited.

The ion-acoustic instability is a current-driven instability. The current along the field lines consists of electrons drifting the ion background. The instability is excited when the combined equilibrium distribution function, consisting of the ion and electron distribution functions, presents somewhere a positive slope where resonance between waves and particles can occur (Treumann et al., p75, 1997). The growth rate of the ion-acoustic instability is strongly dependent on the T_e/T_i ratio. Figure 34 shows the velocity threshold dependence on this ratio.

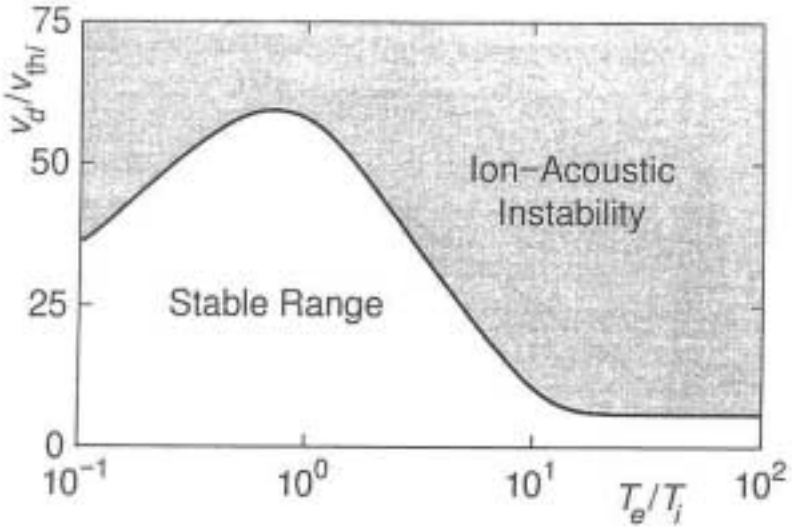

Figure 34: Threshold velocity curve for the ion-acoustic instability.
(from Treumann et al., 1997)

1. Computation of V_d from the field-aligned current.

The Alfven magnetic perturbation is equal to the magnitude of the sheet current K (the current integrated along a direction perpendicular to Io's motion and Jovian field line) flowing between the regions perturbed by Io's motion and the unperturbed regions. For the sake of this estimation, we will assume that this sheet current flows in a structure of about 0.1 R_{Io} but it might be much smaller.

$K=B_y$

$J = K / 0.1\ R_{Io}$

$J = \rho * e * V_d$

$\Rightarrow V_d = B_y / (0.1\ R_{Io} * \rho * e)$

We compute the drift velocity where the ratio B_y/ρ is the largest, close to the ionosphere and get

$V_d \sim 0.0006$ m/s.

2. Computation of T_e and T_i

T_e and T_i are known in the torus close to the Io's orbit. The temperature at the foot of the field line (T_f), close to the ionosphere is unknown. We will make the assumption that the electrons and ions pressure are constant along the field line:

$T_f / T(\text{torus}) = \rho(\text{torus})/\rho_f$

Consequently, the ratio T_e/T_i is constant along the field line, equal to its torus value

$T_e/T_i = 5/60 = 0.1$ and $T_i(\text{torus}) \sim 4{,}000$ eV

Assuming that only protons are found at the foot of the field line (Crary et al., 1996) we compute the thermal velocity of the ions:

$V_{th}^i = (kT_i / m_p)^{1/2} = 450\ 10^3$ m/s

Thus,

$T_e/T_i = 0.1$ and $V_d / V_{th}^i = 10^{-1}$

Figure 34 shows clearly that, because of the relatively high density of ions close to the ionosphere (~ 30 cm^{-3}) and the high ion temperature, the ion-acoustic instability cannot be excited and thus cannot be the source of the anomalous resistivity.

The field-aligned current instability competing most with the ion-acoustic instability is the electrostatic ion-cyclotron instability (Treumann et al., p75, 1997). Figure 35 shows the drift velocity threshold of this instability, normalized to the thermal velocity of the electrons. This

instability is easier to excite than the ion-acoustic mode for T_e/T_i ratio between 0.1 and 10 but the drift velocity that we computed is so small that even this instability cannot be excited.

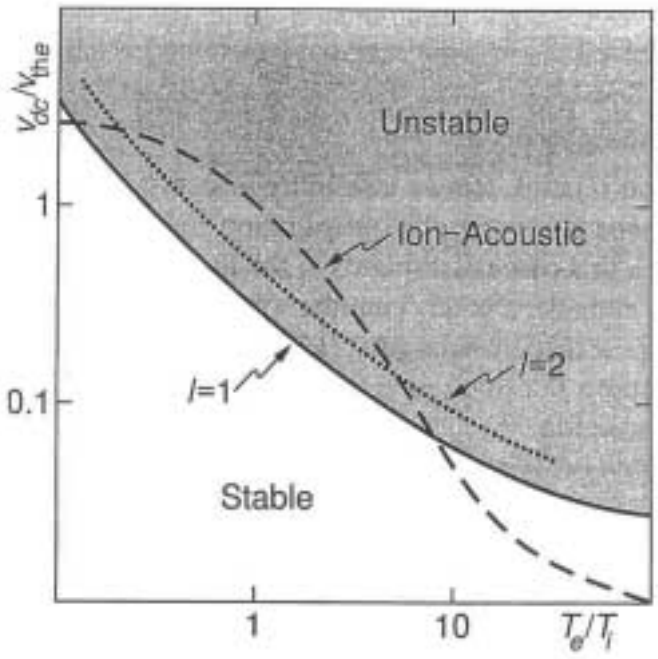

Figure 35: Current drift velocity threshold for the ion-cyclotron instability. (from Treumann et al., 1997)

No instabilities illustrated here can explain the anomalous resistivity along the field lines of Jupiter needed for the formation of $\boldsymbol{E}_{//}$. This means that this parallel electric field is probably formed in very thin filamentary structures that cannot be addressed by this model. At a smaller length scale, some terms that appear in the Generalized Ohm's Law, which were not considered here, like the electron pressure anisotropy (scaling as c/w_{pi}) and of the electron inertia (scaling as c/w_{pe}), might play a role and be the cause of the formation of the parallel electric field.

6. 4. Concept of reconnection rate

In this section, we derive scaling laws for the parallel electric field along the field line. The acceleration mechanism efficiency depends not only on the magnitude of the electric field, but also on the size of the accelerating region where the electric field is applied. Consequently, the magnitude of the electric field is not the most relevant parameter. We show here that the most relevant parameter is the **reconnection rate**. It represents the efficiency of the accelerating mechanism, for it combines the magnitude of the electric field and the size of the region where this electric field is applied. Here, we start by a general definition of the reconnection rate, using the sketch of the reconnection process illustrated in Figure 36. Later on, we will compute the scaling law for the reconnection rate based on the simulation of the Alfven wing propagation discussed in chapter 5.

The magnetic field B^{in} (in Jupiter's case, the Alfven wave magnetic perturbation B_y) is the field that is going to experience reconnection. The field lines of B^{in} are parallel and anti-parallel to the Y-axis. The reconnected field B^{out} is represented by field lines parallel to the Z-axis. The reconnection is caused by an electric field parallel to the X-axis $E_{//}^1$. In the Jupiter example, the X-axis is the direction of the Jovian magnetic field and the parallel electric field $E_{//}^1$ is created by the anomalous resistivity η and the X-aligned current $J_{//}$ due to the B_y perturbation: $E_{//}^1 = \eta J_{//}$. The field lines will reconnect along a reconnection line of length L_1 parallel to the X-axis, along the Jovian magnetic field line. The two planes A and B represent the separatrices that separate the not-yet-reconnected field lines (B^{in} under and above) and the reconnected field lines (B^{out} on the left and on the right). In between the separatrices, we draw a fixed test plane T, with a side of length L_1 along the X-axis, through which we compute the magnetic flux ϕ.

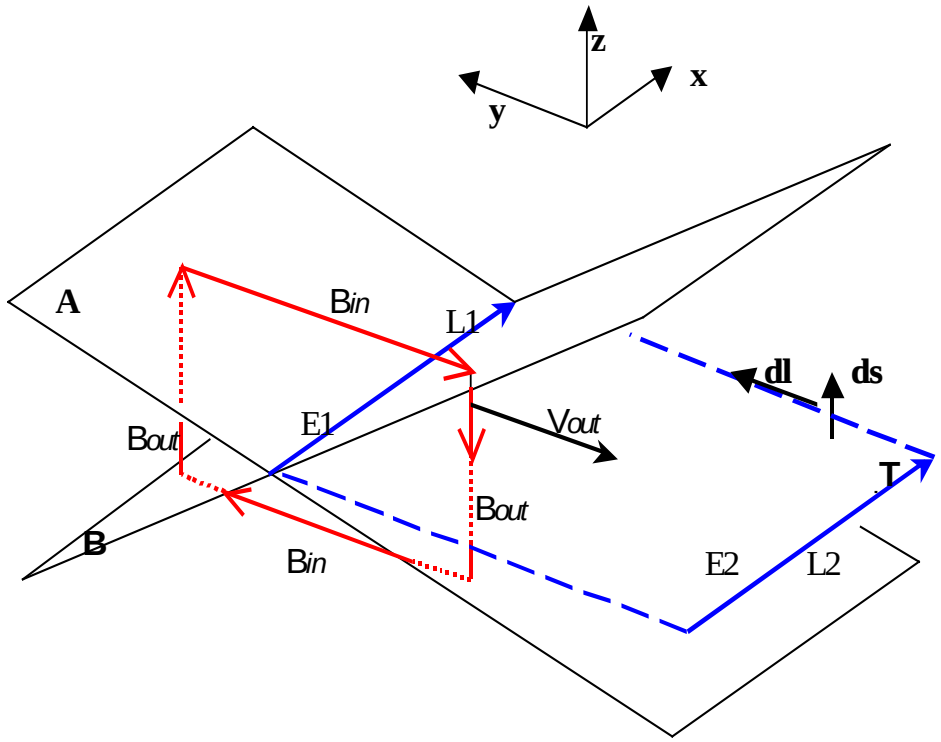

Figure 36: Sketch of the magnetic configuration in a 3D perspective.

- The magnetic flux through the test surface:

$$\phi = \int_T \boldsymbol{B}^{out} \cdot \boldsymbol{ds}$$

The time variation of this flux:

$$\frac{d\phi}{dt} = \int_T \frac{\partial \boldsymbol{B}^{out}}{\partial t} \cdot \boldsymbol{ds}$$

- The reconnection is a process that re-configurate the magnetic topology described by Faraday's law:

$$\frac{\partial \boldsymbol{B}^{out}}{\partial t} = -\nabla \mathrm{x} \boldsymbol{E}_{//}$$

- The variation of the magnetic flux through the test surface:

$$\frac{d\phi}{dt} = -\int_T \nabla \times \boldsymbol{E}_{//} \cdot \boldsymbol{ds} = -\int \boldsymbol{E}_{//} \cdot \boldsymbol{dl}$$

The contribution along the Y–sides of the test surface are =0 (for symmetrical reasons) and the variation of the magnetic flux is

$$\frac{d\phi}{dt} = \int_{L_1} \boldsymbol{E}^2_{//} \cdot \boldsymbol{dl} - \int_{L_2} \boldsymbol{E}^2_{//} \cdot \boldsymbol{dl}$$

- For a steady state reconnection, the variation of the magnetic flux is 0 but there is still reconnecting field lines that go through the test surface. The reconnection rate is defined

$$\Re = \int_{L_1} \boldsymbol{E}^1_{//} . \boldsymbol{dl}$$

In the 1D approach, as the reconnection process cannot be modeled per se, we cannot compute the $E^1_{//} = \eta J^1_{//}$ but we can get an estimation of its variation along the Jovian field line, in other words, we can compute a factor φ_0 scaling as the reconnection rate. Assuming a steady state, $E^1_{//} = E^2_{//}$ and

- $E^2_{//} = u^{out} B^{out}$ in the region where there is no resistivity.
- In the Petscheck description of the reconnection process (see Treumann et al., p149, 1997),

1. u^{out}= the Alfven velocity computed from the B^{in} field:

$$u^{in}_A = \frac{B^{in}}{\sqrt{(\mu_0 \rho^{in})}}$$

2. $B^{out} = \varepsilon B^{in}$ ε is a constant depending on the geometry of the reconnection

thus

$$E^1_{//} = E^2_{//} = \varepsilon u^{in}_A B^{in}$$

As a side comment, it can be understood why we said that the free energy magnitude was, in a first approximation, a measure of the magnitude of the parallel electric field in the simulations showing the propagation of the Alfven wing (section 5.4.2). The parallel electric field scales as

$$E_0 = u_A^{in} B_y = \frac{B_y^2}{\sqrt{(\mu_0 \rho)}}$$

and the free energy as $\propto B_y^2$, but the magnitude of the acceleration parallel electric field depends also on the variation of the plasma density ρ.

- The reconnection rate is thus:

$$\Re = \int_{L_1} \varepsilon u_A^{in} \boldsymbol{B}^{in} \cdot \boldsymbol{dl}$$

The reconnection length L_1 is unknown but it scales as a typical length scale of the field variation. A typical length scale of the magnetic field variation is the radius of the flux tube section of the planetary field B_0 and if we assume that the length of the reconnection region varies like the width of the current sheet, then:

$$L_1 \text{ scales as } \frac{\boldsymbol{1}}{\sqrt{\boldsymbol{B_0}}}$$

.

In summary, the reconnection rate of the Alfven magnetic perturbation scales as

$$\phi_0 \propto L_1 u_A^{in} B^{in} \propto \frac{1}{\sqrt{B_0}} u_A^{in} B_y$$

$$u_A^{in} = \frac{B_y}{\sqrt{(\mu_0 \rho)}}$$

This scaling factor ϕ_0 has the dimension of an electric potential drop. It combines the strength of the parallel electric field and the size of the region where the electric field can accelerate particles and consequently gives information about the efficiency of the acceleration mechanism. We can compute the variation of this scaling factor along the field line, using the 2D

mapping of B_y that was presented in the former chapter. Figure 37 shows the reconnection-rate scaling factor for the 2D mapping of the Alfven magnetic perturbation shown on Figure 27. The conclusion is that the reconnection rate is the largest close to the Jovian ionosphere. Thus, the acceleration mechanism is the most efficient close to the ionosphere.

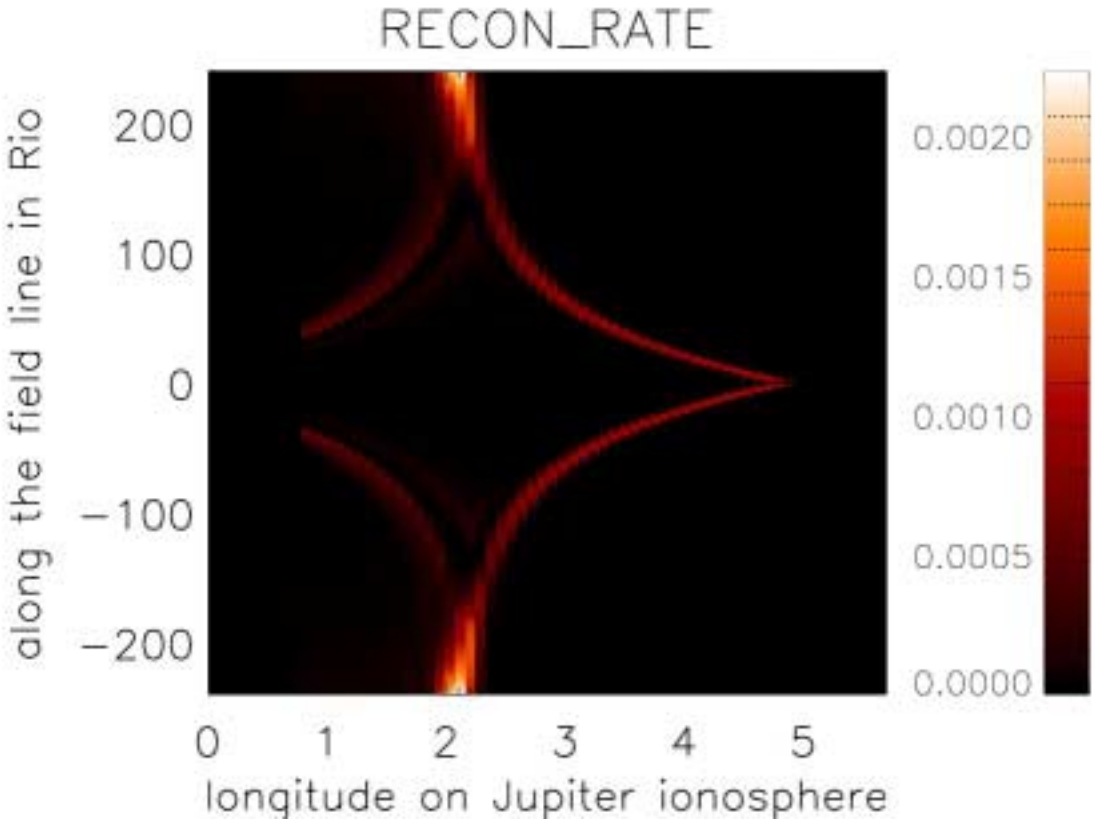

Figure 37: Reconnection-rate variation along field lines

6. 5. Conclusions

From the results above, it seems that the acceleration process is more likely to take place close to the ionosphere, for 2 reasons:

1. Because of the converging-field, the current density is larger close to the ionosphere thus the triggering of anomalous resistivity would be more probable close to the ionosphere.

2. If the resistivity appears anywhere along the field line, the reconnection rate and thus the efficiency of the acceleration mechanism would be larger close to the ionosphere.

These results are surprising: at the end of chapter 5 where we were looking at the free energy only, we were expecting the reconnection to happen preferably close to Io where large Alfven perturbations occur, but the field convergence, the plasma density and the field strength variation along the field lines seem to be in control of the location of the reconnection. Moreover, if the acceleration is close to the ionosphere, then the *observed shift angle* should be close to the *lead-angle* ~ 3^{o}.

1. Even if the resistivity is higher at the ionosphere, that doesn't mean that the resistivity is not high enough to trigger reconnection close to Io at the first place.

2. This 1D approximation doesn't model the reconnection process itself. If reconnection takes place close to Io, then this decoupling close to Io reduces the Alfven magnetic perturbation that keeps on traveling down the ionosphere. If the decoupling is strong, the Alfven magnetic perturbation of the continuing wave might be too small to trigger an anomalous resistivity close to the ionosphere whatever the converging-field effect.

CHAPTER 7: SUMMARY

Recent observations of the Io-related auroral emissions in the Jovian ionosphere confirm that Io strongly interacts with the Jovian magnetic field. The brightness and spectral analyses of these auroral emissions are evidence that an acceleration mechanism is at work somewhere along the field lines connecting Io and Jupiter. This mechanism is still unknown.

The contribution of this thesis is the study, through numerical simulation, of the formation of a localized, parallel, electric field along the Io flux tube that could precipitate particles into the Jovian Ionosphere and cause the auroral emissions. The relative motion of Io in the plasma torus is the source of a magnetic perturbation that propagates along Jupiter's field-lines as an Alfven wave. Accompanying the Alfven wave, a parallel current flows in a current sheet between the field-lines perturbed by Io and the unperturbed field lines on the flanks of Io. We make the assumption that this current can locally trigger an anomalous resistivity if it rises above a critical value. The parallel electric field is locally formed, consistently with Ohm's law: $E_{//}=\eta J_{//}$. This parallel electric field leads to a reconfiguration of the magnetic field-line topology called magnetic reconnection.

In a first step, we study this mechanism with a 3D MHD model and compute the formation of the parallel electric field and the reconnection process self-consistently. It illustrates nicely many features of the Io/Jupiter interaction that are actually observed. These features include the formation of a wake of freshly ionized plasma downstream of Io, the formation of an Alfven wing that propagates from Io to the Jovian ionosphere and the formation of an auroral spot in the Jupiter's ionosphere, at the foot of the field-lines crossing Io. The 3D MHD model has a limited spatial resolution and lacks a realistic description of Jupiter's magnetosphere: the Jovian magnetic field and plasma density are assumed to be uniform along the field-lines crossing Io.

In a second step, we study the effect of a realistic magnetosphere description with a 1D MHD model. The model includes a variable plasma density profile across the torus and the variation of the magnetic field along the field-lines. It is used to compute the Alfven wave perturbation propagating along the field lines crossing Io. It naturally provides a 2D mapping that clearly shows the properties of the Alfven wing formation. This 2D mapping can be extrapolated to a

quasi-3D by interpreting the magnetic perturbation as the sheet current that flows along the Alfven wing, between the field-lines perturbed by Io and the unperturbed field-lines on the flanks of Io frozen to the torus. The 1D approximation lacks the 3D self-consistent dynamics and cannot provide the magnitude of the parallel electric field directly, but we can obtain scaling laws that provide an estimate of the variation of the magnitude of the parallel electric field and of the efficiency of the acceleration mechanism along the field-lines.

The properties of the Alfven wing propagation are correctly analyzed using the 2D mapping. We demonstrate that the ***observed shift angle***, defined as the angle between the auroral Io spot and the instantaneous location of Io projected on the Jovian ionosphere **should be smaller than ~3^{o}**. It is also shown that, because of multiple reflections of the Alfven wave between the torus and the ionosphere, **Io's auroral emission is likely to be structured in multi-spots** separated by a few degrees and that **any change in the Io/Jupiter system** (like a change of Io's location in the torus or density inhomogeneity in the torus) **will cause a change in the structure of the Alfven wing.** This variation of the structure in the Alfven wing **will likely be reflected in the ionosphere auroral emission**. Some evidence of the effect of the Alfven-wing structure on the Io's auroral emissions have been occasionally observed, like a auroral tail emission divided in several distinct spots, multi-arc emissions in the time-frequency DAM spectra or an anticorrelation of the *observed shift angle* of the Io auroral spot in the southern and northern ionospheres. In the first analysis, we use the magnitude of the magnetic perturbation because it provides information about the free energy for the reconnection and acceleration processes. However the free energy, while being important for the relaxation of the system, is not the most relevant parameter for the auroral acceleration.

The formation and efficiency of a parallel electric field accelerating the particles depend on two factors. The first factor is the resistivity or, in general, the onset conditions for a parallel electric field. The formation of the electric field can occur where the parallel current triggers a localized anomalous resistivity somewhere along the magnetic field. We show that because of the converging Jovian magnetic field the most probable location of an anomalous resistivity formation is the region just above the Jovian ionosphere. The second relevant parameter is the reconnection rate. We show that this rate could be interpreted as the efficiency of the acceleration mechanism because it combines the magnitude of the parallel electric field and the size of the acceleration region where the field is applied. In cases of a steady acceleration process this parameter can be interpreted as an electric potential. We show that the reconnection rate is larger

close to the ionosphere. Consequently, the picture resulting from these two factors is that the acceleration process is likely to happen close to the Jovian ionosphere. This conclusion is based on the 1D approximation where the reconnection process itself is not modeled. If reconnection occurs closer to Io then the parallel electric field would reduce the magnetic perturbation that keeps on traveling down to the ionosphere. What is left from the magnetic perturbation would drive a parallel current that might or might not be able to trigger a second accelerating electric field close to the ionosphere. This is an issue that we cannot easily address with this 1D approach.

The observations shows that the Io related emissions are sometimes divided in multi-spots but most of the time are limited to a single spot with an *observed shift angle* varying between 0^0 and 15^0, followed by a long smooth trailing tail covering more than 90^0 of longitude. The model proposed here doesn't address these two features. An easy way would be to blame the observations for their lack of reliability: The measurement of the *observed shift angle* is based on a magnetic field model whose high orders multipoles are poorly constrained. The smooth tail might be structured as a succession of close spots that the instruments are currently unable to resolve. It is also important to note that the physics at work in the Io/Jupiter system is more complicated than the 1D picture presented here. Some of the issues might be relatively easy to address by a closer look at the 3D: The long auroral tail might result from parallel currents flowing along a long wake of freshly ionized neutrals downstream of Io. These currents might trigger the formation of an extended structure of parallel electric field that accelerate electrons in an extended auroral tail behind the Io spot. We are confident that future high-resolution observations of the Io's related aurora will provide a wealth of structure, which may in particular resolve some of the mapping issues of this aurora.

REFERENCES

Acuna, M. H., F. M. Neubauer, N. F. Ness, Standing Alfven wave current system at Io: Voyager 1 observations, J. Geophys. Res., **86**, 8513, 1981.

Acuna, M. H., K. W. Behannon, J. E. P. Connerney, Jupiter's magnetic field and magnetosphere, in *Physics of the Jovian magnetosphere*, edited by A. J. Dessler, pp. 1-50, Cambridge University Press, New York, 1983.

Bagenal, F., and J. D. Sullivan, Direct plasma measurements in Io torus, J. Geophys. Res., **86**, 8447, 1981.

Bagenal, F., Empirical model of the Io plasma torus: Voyager measurements, J. Geophys. Res., **99**, 11043, 1994.

Bagenal, F., The ionization source near Io from Galileo wakes data, Geophys.Res.Lett., **24**, 2111, 1997.

Belcher, J. W., The low-energy plasma in the Jovian magnetosphere, in *Physics of the Jovian magnetosphere*, edited by A. J. Dessler, pp. 68-105, Cambridge University Press, New York, 1983.

Birk, G. T., and A. Otto, A three-dimensional plasma-neutral gas-fluid code, Computer Physics Communication, **125**, 513, 1995.

Clarke, J. T., G. E. Ballester, J. T. Trauger, R. Evans, J. E. P. Connerney, K. Stapelfeldt, D. Crisp, P. D. Feldman, C. J. Burrows, S. Casertano, J. S. Gallagher III, R. E. Griffiths, J. J. Hester, J. G. Hoessel, J. A. Holtzman, J. E. Krist, V. Meadows, J. R. Mould, P. A. Scowen, A. M. Watson, J. A. Westphal, Far-ultraviolet imaging of Jupiter's aurora and the Io footprint, Science, **274**, 404, 1996.

Clarke, J. T., G. Ballester, J. Trauger, J. Ajello, W. Pryor, K. Tobiska, J.E.P. Connerney, G. R. Gladstone, J. H. Waite Jr., L. Ben Jaffel, J. C. Gerard, Hubble Space Telescope imaging of Jupiter's aurora during the Galileo orbiter mission, J. Geophys. Res., **103**, 20217, 1998.

Connerney, J. E. P., M. H. Acuna, N. F. Ness, Modeling the Jovian current sheet and inner magnetosphere, J. Geophys. Res., **86**, 8370, 1981.

Connerney, J. E. P., Doing more with Jupiter's magnetic field, in *Planetary Radio Emission III*, pp. 13-33, edited by H.O. Rucker, S.J. Bauer and M.K. Kaiser, Austrian Acad. Sci., Vienna, 1992.

Connerney, J. E. P., M. H. Acuna, N. F. Ness, T. Satoh, New models of Jupiter's magnetic field constrained by the Io flux tube footprint, J. Geophys. Res., **103**, 11929, 1998.

Connerney, J. E. P., and T. Satoh, the H_3^+ ion: a remote diagnostic of the Jovian magnetosphere, Phil. Trans. R. Soc. Lond., **358**, 2471, 2000.

Crary, F. J., F. Bagenal, J. A. Ansher, D. A. Gurnett, W. S. Kurth, Anisotropy and proton density in the Io plasma torus derived from whistler wave dispersion, J.Geophys. Res., **101**, 2699, 1996.

Crary, F. J., On the generation of an electron beam by Io, J. Geophys. Res., **102**, 37, 1997.

Crary, F. J., and F. Bagenal, Coupling the plasma interaction at Io to Jupiter, Geophys. Res. Lett., **24**, 2135, 1997.

Dessler, A. J., *Physics f the Jovian Magnetosphere*, edited by A.J. Dessler, Cambridge Univ. Press, New York, 1983.

Dols, V., J. C. Gerard, J. T. Clarke, J. Gustin, J. Grodent, Diagnostics of the Jovian aurora deduced from ultraviolet spectroscopy: Model and HST/GHRS observations, Icarus, **147**, 251, 2000.

Goertz, C. K., Io's interaction with the plasma torus, J. Geophys. Res., **85**, 2949, 1980.

Glodreich, P., and D. Lynden-Bel, Io a Jovian unipolar inductor, Astroph. J., **156**, 59, 1969.

Hill, T. W., A. J. Dessler, C. K. Goertz, Magnetospheric models, in *Physics of the Jovian magnetosphere*, edited by A. J. Dessler, pp. 353-394, Cambridge University Press, New York, 1983.

Khurana, K. K., M. G. Kivelson, C. T. Russel, Interaction of Io with its torus: Does Io have an internal magnetic field, Geophys. Res. Lett., **24**, 2391, 1997.

Kopp, A., Modifications of the electrodynamic interaction between Jupiter and Io due to mass loading effects, J. Geophys. Res., **101**, 24943, 1996.

Neubauer, F. M., Nonlinear standing Alfven wave current system at Io: theory, J. Geophys. Res., **85**, 1171, 1980.

Roesler, F. L., H. W. Moos, R. J. Oliversen, R. C. Woodward Jr., K. D. Retherford, F. Scherb, M. A. McGrath, W. H. Smyth, P. D. Feldman, D. F. Strobel, Far-ultraviolet imaging spectroscopy of Io's atmosphere with HST/STIS, Science, **283**, 353, 1999.

Otto, A., and G. T. Birk, Formation of thin auroral arcs by current striation, Geophys. Res. Lett., **20**, 2833,1993.

Prange, R., D. Rego, D. Southwood, P. Zarka, S. Miller, W. Ip, Rapid energy dissipation and variability of the Io-Jupiter electrodynamic circuit, Nature, **379**, 323, 1996.

Prange, R., D. Rego, L. Pallier, J. E. P.Connerney, P. Zarka, J. Queinnec, Detailed study of FUV Jovian auroral features with the post-Costar HST faint object camera, J. Geophys. Res., **103**, 20195, 1998.

Smyth, W. H., Neutral cloud distribution in the Jovian system, Adv. Space Res., **12**, (8)337, 1992.

Southwood, D. J., M. G. Kivelson, R. J. Walker, J. A. Slavin, Io and its plasma environment, J. Geophys. Res., **85**, 5959, 1980.

Thorne, R. M., Microscopic plasma processes in the Jovian magnetosphere, in *Physics of the Jovian magnetosphere*, edited by A. J. Dessler, pp. 454-488, Cambridge University Press, New York, 1983.

Treumann, R. A., and W. Baumjohann, *Advanced Space Plasma Physics*, 381 pp., Imperial College Press, London, 1997.

Wong, M. C., W. H. Smyth, Model calculation for Io's atmosphere at eastern and western elongations, Icarus, **146**, 60, 2000.

Wright, A. N., The interaction of Io's Alfven waves with the Jovian magnetosphere, J. Geophys. Res., **92**, 9963, 1987.